Paulo André Matos Ribeiro Martins

Bachelor Degree in Biomedical Engineering Sciences

Cuffless Blood Pressure Estimation

Dissertation submitted in partial fulfillment
of the requirements for the degree of

Master of Science in
Biomedical Engineering

Co-advisers: Inês Sousa, PhD, Fraunhofer AICOS
Pedro Manuel Vieira, Assistant Professor, FCT-UNL

Examination Committee

Chairperson:	Prof. Dr. Valentina Borissovna Vassilenko
Raporteur:	Prof. Dr. Carla Maria Quintão Pereira
Member:	Prof. Dr. Pedro Manuel Cardoso Vieira

FACULDADE DE
CIÊNCIAS E TECNOLOGIA
UNIVERSIDADE NOVA DE LISBOA

September, 2019

Cuffless Blood Pressure Estimation

This document was created using the (pdf)LaTeX processor, based in the "novathesis" template[1], developed at the Dep. Informática of FCT-NOVA [2].
[1] https://github.com/joaomlourenco/novathesis [2] http://www.di.fct.unl.pt

PP...

Acknowledgements

First and foremost, I would like to express my special gratitude to my supervisor Phd. Inês Sousa, who gave me all the support, guidance, and help throughout the whole project. But, more important, my deep and sincere gratitude for never letting me settle, always challenging me to try new things. I will define the concept of "excellent advisor" after this experience. I would also like to thank my advisor Professor Pedro Vieira, who made this dissertation possible and for always helping me when I needed.

Besides my advisors, I would like to thank Fraunhofer AICOS as a whole for all the support, material, conditions, and the opportunity to work on my dissertation in an excellent environment. I am amazed with the outstanding work developed in this institution. A very special thanks to everyone in Lisbon for welcoming me so well, I felt at home. I would truly like to highlight my colleagues Leticia, Sara, João, Az (made in azores), *informático* 1 and 2, I really enjoyed working next to you.

À minha familia, especialmente aos meus pais e irmão, um muito obrigado por me terem tornado a pessoa que sou hoje, foram fundamentais em todo o meu percurso académico e não académico, e sei que, sem o vosso apoio seria tudo bastante mais difícil, ou mesmo impossível.

And last but not least, a whole paragraph to thank Ana Pi, you were fundamental during all this time, thank you for all the help not only in this dissertation.

Abstract

The blood pressure is an important factor in the diagnosis and evaluation of several diseases, such as acute myocardial infarction and stroke. This way, continuous monitorization of this parameter is crucial to a correct health evaluation. The current methods, like the oscillometric method, have some major drawbacks, that can influence the output values or even make the measurements impossible. One example is the high frequency evaluation of the blood pressure, in the standard used methods the process of measuring can take up to 3 minutes, and a waiting time is necessary between consecutive measurements.

This dissertation presents two different cuffless solution to solve those problems. One based on physical models of the human body, and the other using machine learning techniques.

In the first solution seven models that correlate pulse transit time and blood pressure, deducted by different authors, were tested to evaluate which one performed better. The testes were performed in a custom dataset acquired at Fraunhofer AICOS and in clinical environment, with two different devices (low cost device and medical grade device). The results indicate that pulse transit time can be used to track blood pressure, the developed device/method was evaluated as grade A based in the Standard IEEE 1708-2014.

The second solution it's a proof of concept using a public database and three different machine learning methods (Random Forest, Neural Network and AdaBoost). Two sets of features are calculated from the ECG and PPG signals, one using TSFEL (spectral, frequency and time domain features) and a total of 15 custom features. The proposed method outperforms the methods presented in bibliography with mean absolute error of 3.6 mmHg and 2.0 mmHg to systolic and diastolic blood pressure respectively.

Keywords: Blood Pressure, Cuffless, Machine Learning, Physiological Models, Photoplethysmography, Electrocardiogram, Signal Processing

Resumo

A pressão arterial é um fator importante no diagnóstico e avaliação de diversas doenças, como o enfarte agudo do miocárdio e o ataque cardíaco. Assim, uma avaliação contínua deste parâmetro é fundamental para uma boa avaliação clínica. Os métodos atuais, como o método oscilométrico, apresentam algumas desvantagens, que podem influenciar e/ou impossibilitar a medição da pressão arterial, um exemplo disso é a medição da variações rápidas deste parâmetro fisiológico. Nos métodos comumente utilizados, o processo de medição pode demorar até 3 minutos e um período de espera entre medições é bastante aconselhado.

Nesta dissertação são apresentadas duas soluções para resolver estes problemas, um tendo como base modelos do corpo humano, e outro usando técnicas de *machine learning*.

Na primeira solução, sete modelos deduzidos por diferentes autores, foram testados para avaliar qual deles apresenta melhor desempenho. Os testes foram realizados num conjunto de dados adquiridos na Fraunhofer AICOS e em ambiente clínico, com dois dispositivos diferentes (dispositivo de baixo custo e dispositivo de *grade* médico). Os resultados indicam que o tempo de trânsito do pulso pode ser usado para estimar a pressão arterial. O dispositivo/método desenvolvido foi avaliado com grau A com base no standard IEEE 1708-2014.

A segunda solução é uma prova de conceito usando a base de dados MIMIC III e três métodos diferentes de aprendizagem automática (*Random Forest*, Redes neuronais e *AdaBoost*). Dois conjuntos de *features* são calculados a partir dos sinais de ECG e PPG, um usando TSFEL (*features* de domínio espectral, frequência e tempo) e um total de 15 *features* personalizadas. O método proposto apresenta resultados superiores aos métodos descritos na bibliografia com erro médio absoluto de 3,6 mmHg e 2,0 mmHg referente, respetivamente, à pressão arterial sistólica e diastólica.

Palavras-chave: Pressão Arterial, Aprendizagem Automática, Modelos Fisiológicos, Fotopletismografia, Eletrocardiograma, Processamento de Sinais

Contents

List of Figures

List of Tables

Acronyms

AdaBoost adaptive boosting.

ADC analog to digital converter.

BP blood pressure.

BPM beats per minute.

BVP blood volume pulse.

DBP diastolic blood pressure.

DTW dynamic time warping.

ECG electrocardiogram.

FIR finite impulse response.

HBP high blood pressure.

HR heart rate.

IAP intra-arterial pressure.

LSTM long-and short term memory networks.

MAE mean absolute error.

MAP mean arterial pressure.

ME mean error.

MIMIC medical information mart for intensive care.

NN neural network.

PAT pulse arrival time.

PCA principal component analysis.

PEP pre-ejection period.

PIR photoplethysmogram intensity ratio.

PP pulse pressure.

PPG photoplethysmography.

PTT pulse transit time.

PTT_{init} initial pulse transit time.

PTT_{max} maximum pulse transit time.

PTT_{onset} onset pulse transit time.

PWV pulse wave velocity.

RF random forest.

RMSE root mean squared error.

RRSD RR standard deviation.

SBP systolic blood pressure.

SD standard deviation.

TSFEL time series feature extraction library.

Chapter 1

Introduction

The health care subject and the technology in medicine have increasingly gain importance in the society. One of the objectives (and trends) in the biomedical investigation field is to develop mechanisms and technology that can push diagnostic and treatment forward, and make them easier and available for the masses.

In this chapter several topics will be addressed to explain and present the importance and need of a new method to measure the BP without a cuff.

1.1 Context and Motivation

The high blood pressure (HBP), also called hypertension, is a significant risk factor in several cardiovascular diseases [1], such as acute myocardial infarction and stroke. According to data from the World Health Organization, it is estimated that 13% of the world's deaths are directly or indirectly linked to HBP, compared to 9% associated with, smoking [2]. In Portugal, the numbers are very worrying, given that it is estimated that approximately 36% of the population suffers from hypertension [3].

The BP measurement is therefore essential throughout the diagnostic and evaluation process of hypertension, and the control of this parameter is fundamental during surgeries and in ambulatory. Currently, the most commonly used and the gold standard method is auscultation using a mercury sphygmomanometer or an electronic equivalent. By hearing the Korotkoff sounds, it is possible for the physician to identify the systolic blood pressure (SBP) and diastolic blood pressure (DBP) [5]. The measurement of BP through the method described above is simple and presents values, in most cases, sufficient for a correct diagnosis [6]. However, there are some limitations inherent to this method, such as the discomfort associated with increased pressure in the cuff, which may

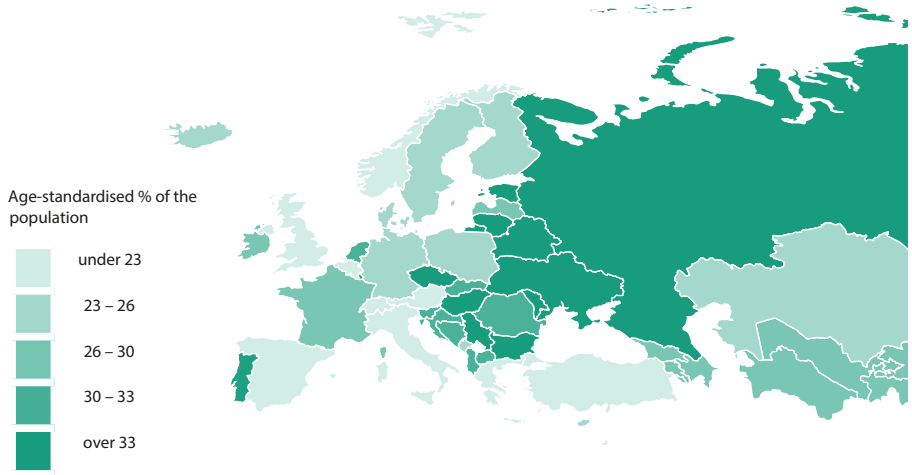

Figure 1.1: Prevalence of raised BP, aged 18+ years, males, 2014, Europe, adapted from [4]

lead to the incorrect BP measurements due to the patient's stress conditions [7], the impossibility of realizing continuous beat-to-beat measurements to evaluate high frequency changes in BP, since the whole process of inflation, deflation, and stabilization can take between one and two minutes [8, 9], or even the presence of the physician/ nurse, that can lead to a white coat hypertension condition. This is a phenomenon that affects 15% to 30% of the subjects [10], and it is characterized by an abnormal increase in BP only in clinical environment, that can contribute to a false positive hypertension diagnosis. It is also difficult to measure BP during sleep since the patient can be awakened due to inflation of the cuff, which means that the values are not representative of what is intended to be evaluated [9].

Some of this limitations can be solved by measuring intra-arterial pressure (IAP). Such a procedure involves the insertion of a catheter into the artery, usually the radial artery [11] and the measurement of the BP continuously. Since this is an invasive method, it is associated with the usual risks of this kind of procedures, such as infection and thrombi formation [11], but also pain and discomfort.

Due to technology development, other methods to measure BP based on pulse transit time (PTT) and pulse wave velocity (PWV) attempt to solve these gaps in the currently used methodologies, so that a all place, correct, continuous and comfortable BP measurements are possible.

1.2 Objectives

The objective of this dissertation is to develop a system/method to estimate BP without the cuff that is usually used in the current methods.

Two different approaches have been proposed during the years, one based on the

physical modulation of the blood flow in the arteries, and the other base on machine learning techniques. This work aims to evaluate the differences between these two approaches, and compare them with previous works in the area. Several sub-objectives can be identified in both parts of this work:

- **Physical Models:** It can be decomposed in four different, but not independent phases. The first phase is the setup of the acquisition system, some important aspects should be tested, like which physiological signals to acquire, the accuracy and scalability of the system, and the possibility to be adapted to a current day-to-day use by everyone in different environments and situations. Two systems with different price points are also evaluated in this dissertation, a low cost device and a medical grade device, to evaluate the influence of the acquisition system in the overall accuracy. The second phase is the signal acquisition and processing phase, at this stage is important to identify some sub objectives, like for example, the signals digital filtering, the test of different algorithms to automatic identify important fidutial points in the acquired physiological signals and implementation of the algorithm to calculate PTT. The third phase consists of the BP estimation algorithms implementation, the objective is to use the pairs (PTT,BP) to train different models deducted using physical properties of the blood flow in vessels and use those models to predict future values of BP. The fourth and last phase is data acquisition procedure, the objective is to acquire good quality data that will be used to evaluate each system and model. Several factors need to be taken into account and studied, like the procedure to vary the BP in the calibration process and the acquisition protocol.

- **Machine Learning:** This approach will be developed as a proof of concept, with the objective of testing the BP estimation possibility based in machine learning techniques.

The expected output will be the order of magnitude of the measurement error of different cuffless BP estimation methods against the cuff-based methods. This work should provide useful information for future projects related to the cuffless BP measurements.

1.3 Applications

The work developed in this dissertation has the possibility to be used in several aspects of the medical and biomedical field.

One strong example is the growth in the demand of wearable devices that evaluate health and physical condition during the day or during physical activities. The most common devices use several sensors to give the user usefull information like number of steps, active time, travelled distance, heart rate, stress level, oxygen saturation and, more recently, the ECG signal. A method to passively measure the BP without using a cuff can

be implemented in this format allowing the user to track this important parameter of his health.

This method can also be a better and more comfortable approach to measure BP in a ambulatory scenario, since the normal devices to measure this physiological parameter in this conditions are relatively bulky, uncomfortable and can influence the measurements in some conditions, like during sleep, where the inflation and deflation of the cuff can wake up the subject.

1.4 Thesis Outline

This work is structured as follows:

- **Chapter 2:** The objective of this chapter is to present and explain with sufficient detail, concepts that are useful to a complete understanding of this dissertation, like the definition of the BP concept, the origin on the PPG and ECG signal, among others;
- **Chapter 3:** The objective of this chapter is to describe the materials and methodologies used in the physical model approach to estimate BP
- **Chapter 4:** Just like in chapter 3, the objective of this chapter is to describe materials and methodologies used to estimate BP using machine learning.
- **Chapter 5:** The core objective in this chapter is to compare both models, make considerations, and propose future adaptations that can be implemented in the future to improve the process of BP estimation without cuff.

CHAPTER 2

Background Concepts

TO a correct understanding of this work it is important to define and explain several definitions, and concepts. This includes the definition of BP, explanation of some physiological signals, algorithms to detect important points in those signals, machine learning methods, among others.

2.1 Blood Pressure

2.1.1 Definition

In a general sense, the pressure is a force per unit area, so BP is defined as the force that blood exerts in blood vessels inner walls divided by area of that vessel's inner walls. The maximum pressure occurs during ventricular systole and is called systolic blood pressure and the minimum pressure occurs during ventricular diastole and is called diastolic blood pressure (Figure 2.1). The mmHg unit (millimeters of mercury) is commonly used in medicine rather than the SI unit, the pascal. As the name indicates a pressure corresponding to 120 mmHg would be equal to the pressure felt at the column base with 120 mm of mercury height. It is important to note that blood pressure measurement is measured in relation to atmospheric pressure [12].

Therefore the BP varies continuously during the blood flow as shown in Figure 2.1, two pressure points have especial relevance for medical diagnosis, the SBP, that is the maximum pressure that occurs during systole, and DBP, that is the minimum pressure that occurs during diastole.

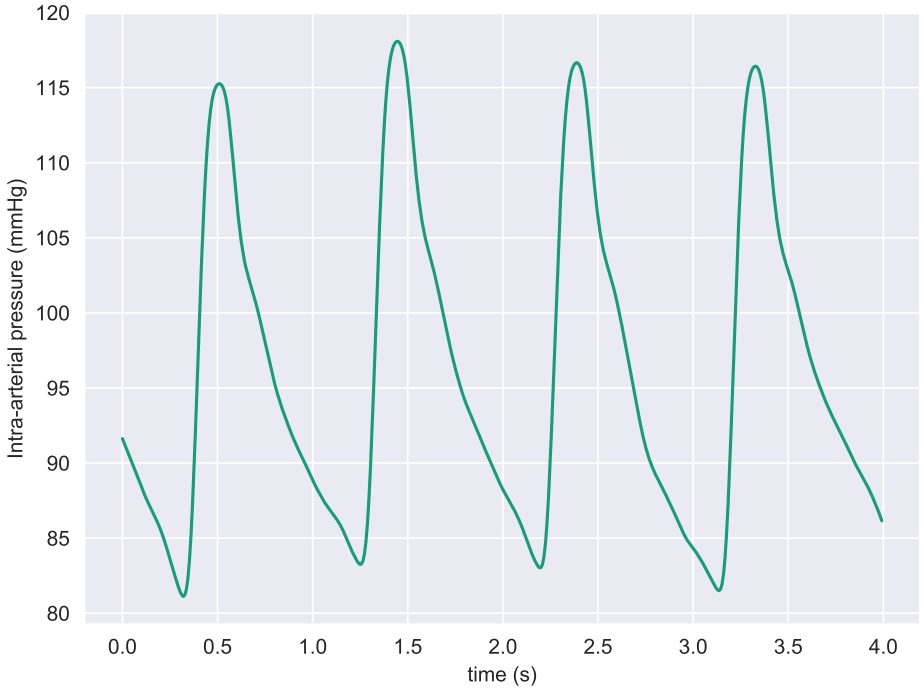

Figure 2.1: Continuous BP signal

2.1.2 Mean Arterial Pressure

The mean arterial pressure (MAP) is a critical hemodynamic factor, fundamental for a correct evaluation of blood perfusion in critically ill patients [13]. The MAP can be estimated with SBP and DBP, through equation 2.1 [14].

$$MAP = \frac{2}{3}DBP + \frac{1}{3}SBP \tag{2.1}$$

2.1.3 High blood pressure

The table 2.1 summarizes the BP classification for adults, according to data from the European Society of Hypertension.

Different organizations define their own classes of BP classification values, and because of this factor it is common to find slightly different values and/or classifications.

2.1.4 Pulse Pressure

The PP is defined as the pressure difference between the SBP and the DBP (Figure: 2.2) and it is influenced mainly by two factors, stroke volume and vascular compliance [17].

The pulse of pressure caused by the blood output from the heart, associated with the elastic properties of the arteries, leads to the distension of these vessels so as to temporarily accommodate the ejected blood, storing energy that is subsequently used for

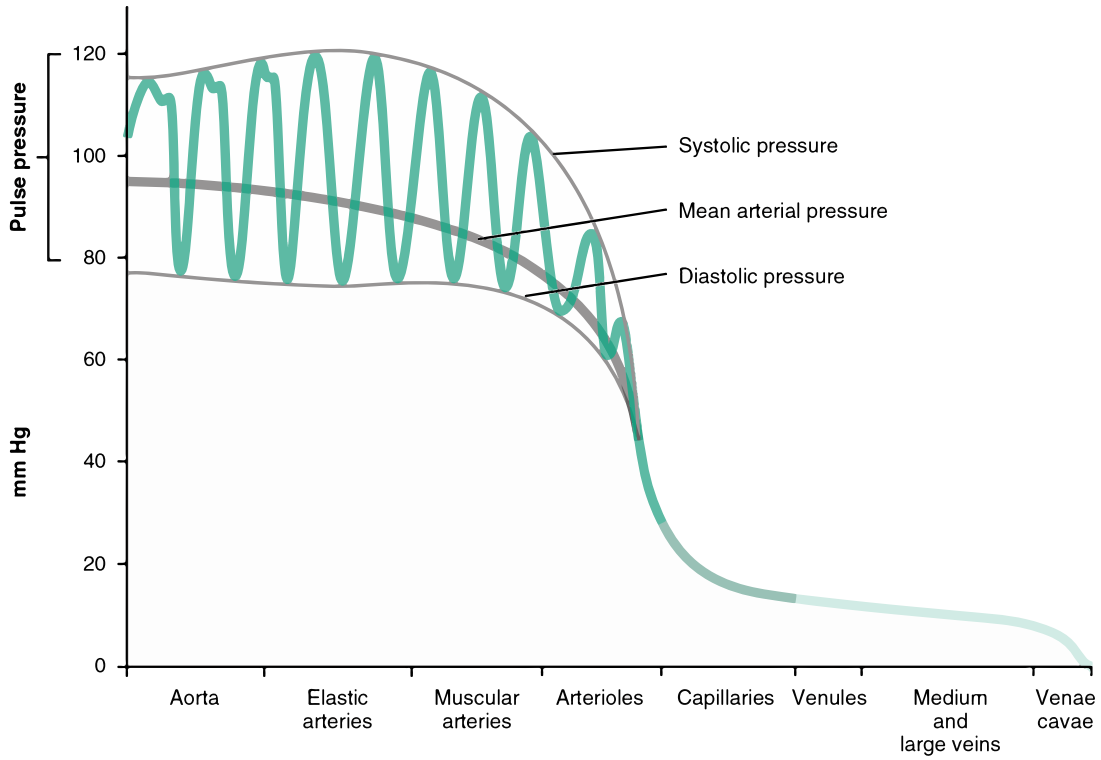

Figure 2.2: BP along the different blood vessels, and representation of MAP and the pulse pressure (PP) [15]

Table 2.1: Reference BP values according to the ESH [16]

Classification	**SBP (mmHg)**		**DBP (mmHg)**
Great	<120	AND	<80
Normal	120 to 129	OR	80 to 84
Normal High	130 to 139	OR	85 to 89
Hypertension grade 1	140 to 149	OR	90 to 99
Hypertension grade 2	150 to 179	OR	100 to 109
Hypertension grade 3	$\geqslant$ 180	OR	$\geqslant$ 110

the blood movement maintenance in the diastolic phase, ensuring a relatively continuous blood flow in the tissues [18].

This momentary increase in the artery volume can be detected in various body parts, such as the common carotid artery, the radial artery, among others, simply by the palpation method.

2.1.5 Traditional Methods to Measure Blood Pressure

To understand the differences between the proposed methods in this work and the commonly used methods it is important review the most common tradional method to measure the BP.

2.1.5.1 Invasive method

Invasive blood pressure monitoring is a technique that involves a direct blood pressure measurement inside an artery, commonly used during surgeries or in the Intensive Care Unit. A catheter needs to be placed inside the patient's artery, usually brachial, radial or femoral artery and connected to an electronic pressure sensor.

This method is considered the most accurate method to measure blood pressure [19], and, more important, to do a continuous beat-to-beat measurement of the value with a correct visualization of the signal waveform, useful, for example, in vascular surgeries. Since it is an invasive process, there is a risk of some complications, like infection, pain, thrombosis, bleeding, and others.

2.1.5.2 Palpatory method

The palpatory method is a simple method that can be used to estimate systolic blood pressure. The cuff is placed on the patient arm and inflated until the pressure inside the cuff is 30 to 40 mmHg higher than pressure where no pulse can be felt, then the cuff is slowly deflated, the systolic pressure is the pressure point where pulse wave can be felt again.

This method requires tactile sensibility and experience by who performs it, and it usually underestimates the systolic blood pressure.

2.1.5.3 Auscultatory method

In this noninvasive method a cuff is connected to a manometer and is placed around the patient's arm, just above the elbow, and a stethoscope is held in a distal position over the brachial artery.

The BP measurement using mercury sphygmomanometer is considered the gold standard in the subject, however, this kind of sphygmomanometer is being discontinued, and their use discouraged due to the harmful characteristics of mercury.

Aneroid manometers came as a solution to this problem because no mercury is used. They have a purely mechanical mechanism with metal bellows that expand when the pressure in the cuff increases [20]. This mechanism has some drawbacks: it is just accurate if adequately calibrated [21], needs maintenance every six months, and needs to be handled gently, because it is easily de-calibrated [20]. This sort of devices is, in general, less accurate than mercury sphygmomanometers.

More recent developed sphygmomanometers, called hybrid sphygmomanometers, use a mix of both electronic and auscultatory features [22]. In this genre of devices, the mercury column is replaced with an electronic pressure gauge, and BP is taken in the same process as with the other two devices, having the advantage that any terminal digit preference (when the observer rounds of a measurement) are made [22].

BP measurement using the auscultatory method follows the following steps:

- The cuff is inflated until the pressure inside the cuff exceeds the pressure in the artery, leading to a total collapse of the brachial artery, at this point no sound can be heard in the stethoscope because blood cannot flow through the area constricted by the cuff.

- Then the pressure is slowly reduced

- At some pressure point, a periodic sound can be heard in the stethoscope, known as Korotkoff sounds. They result from the vibration produced by the flowing blood in the semi constricted area. It is important to note that Korotkoff sounds change tone and loudness with the pressure reduction inside the cuff [20], five phases can be usually identified, phase I, associated with clear tapping sound start, phase II, when the sounds become softer and more extended, phase III, defined when the sounds become crisper and louder, phase IV, when the sounds become muffled and softer, and phase V, when no sound can be detected [23].

- Several studies conclude that the pressure related to the starting sound in phase I is associated with systolic pressure, however, the value usually is lower than the real physiological value [24]. Therefore, systolic pressure tends to be underestimated.

- Phase V can be linked to diastolic blood pressure, but usually, the measured value is higher when compared to intra-arterial pressure [24].

Despite the BP differences between auscultatory method and intra-arterial method, the auscultatory method provides adequate data for various applications in medicine. However, it has some drawbacks that limit the use of this technique in some specific situations. First, it is not possible to do a continuous measurement, since the procedure of inflation and deflation, take some time. A second measurement should not be done right after the first one. To avoid errors in the measurement is necessary to do a pause of one or two minutes between them [25], because of this, a short-term study in BP variation is not possible. Long-term studies, mainly during the night, are also hard to implement, since the process (inflation and deflation of the cuff) will probably disturb the patient, and the value measured do not represent the true BP value at that time. Another problem is the influence of the measurement itself or the ambient where it is made, on the patient's blood pressure [9].

2.1.5.4 Oscillometric method

The oscillometric method, employed by most clinical-grade automated BP devices, takes advantage of cuff pressure variations that append due to the blood pressure itself. This method was first demonstrated in 1876 by the French scientist Étienne-Jules Marey in "Pression et vitesse du sang".

In this method, just like in the auscultatory method, the cuff is inflated until the pressure is higher than systolic pressure, then it is slowly deflated to a sub- diastolic pressure level. The pressure signal inside the cuff is recorded during deflation and then filtered to remove the low-frequency component. Several studies indicate that the point of maximum oscillation appears to provide an acceptable value to the mean arterial pressure [26]. Systolic and diastolic blood pressure can be estimated using mean arterial pressure and empirically derived algorithms and oscillometric models, such as the fixed-ratio method [27].

This method has some advantages when compared with auscultatory one [23]:

- The person that is doing this evaluation does not need to know the exact location of the brachial artery since no sound needs to be heard. Therefore, the patient can do it alone in ambulatory;
- The possibility to be used in patients with muted Korotkoff sounds;
- It is less susceptible to external noise.

However, this technique has some disadvantages, such as mean arterial pressure underestimation in patients with stiff arteries and wide pulse pressures. This happens because oscillations amplitude have a direct correlation with these factors [23]. Other disadvantages can be pointed out, as the high sensitivity to motion artifacts [23] and, in some cases, reduced accuracy due to the empirical estimations of systolic and diastolic blood pressure.

2.1.5.5 Ultrasound technique

This method, proposed in 1965 by Ware, is based on the Doppler effect. This physical phenomenon can be explained as a change in a wave frequency when the font has a relative motion to an observer. The Doppler effect can be used to obtain a systolic and diastolic blood pressure, this last one with higher uncertainty [28].

Just like in oscillometric, auscultatory and palpatory method, an inflatable cuff is placed around patient harm, with an ultrasound transducer over the brachial artery, the cuff is then inflated until the artery collapse, at this point, since there is no blood flowing through the vessel, any change in frequency can be detected, because the artery wall is not in motion. Thereafter the cuff pressure is slowly deflated, at the precise moment that cuff pressure becomes smaller than systolic pressure, the artery opens with high velocity [29], this motion causes a start in the ultrasound frequency shift signal. When the cuff

pressure falls below diastolic pressure, a characteristic muffled signal can be detected in the ultrasound frequency shift signal, "marking" the diastolic pressure [29]. After that other high-frequency signals can be detected due to the usual wall motion caused by wave pressure [29].

Ultrasound technique can be used to measure, with good accuracy, systolic blood pressure value in infants and children, as well as in patients with faint Korotkoff sounds [23].

2.1.5.6 Vascular unloading method

This method, also known as Finapres (from FINger Arterial PRESsure), the name of the commercial equipment, based in the work of Czech physiologist Jan Peñáz, uses the infrared light transmission to measure blood pressure in the finger [23].

A cuff with a photo-plethysmograph is placed around the finger, and a first calibration is made [30]:

1. The cuff is inflated until a pressure level below normal blood pressure (P_i);
2. The photo-plethysmograph signal is recorded during several cardiac cycles ($I(t)$);
3. The cuff pressure (P_i) is increased in small increments, and the point 2 repeated to each pressure;
4. The cuff pressure is then fixed to the pressure value that maximize the $I(t)$ amplitude, and the mean light intensity (I_{mean}) is calculated over several heart cycles.

Then the measurement process begins, a pressure servo regulator dynamically changes P_i so that the I_{mean} stays constant, the pressure inside the cuff represents the blood pressure at that time. Several studies support the high correlation between the cuff pressure P_i and the blood pressure at that time [30, 31].

This method makes possible the blood pressure measurement in real time in a non-invasive way. However, this equipment is typically used scientific research because of the high retail price, around 40 000 US dollars.

2.1.5.7 Tonometry

Just like the vascular unloading method, the tonometry can measure in a not invasive and continuous way the blood pressure. In this technique, the artery (usually radial artery [32]) is flattened due to a force applied by a cuff, or a strap, without occlusion. The artery should be supported from below by a bone [33] (typically the radial bone [32]).

A force sensor or an array of sensors can be used to measure the force applied by the artery wall. This force has a direct correlation with intra-arterial blood pressure when some specific conditions are satisfied [32]:

- The artery us supported by the bone or other hard structure;

- The artery cannot be occluded, if this happens the measurement will be erroneous[33];
- The artery wall thickness is much larger than the skin thickness;
- The artery wall beaves like an ideal membrane, where only the tensile force is transmitted;
- The arterial rider (Figure 2.3) is smaller than the flattened area and is centered over it;
- And the string constant of the transducer is much higher when compared with artery string constant.

In these conditions, theoretically proved [34], the force signal is directly proportional to intra-arterial blood pressure.

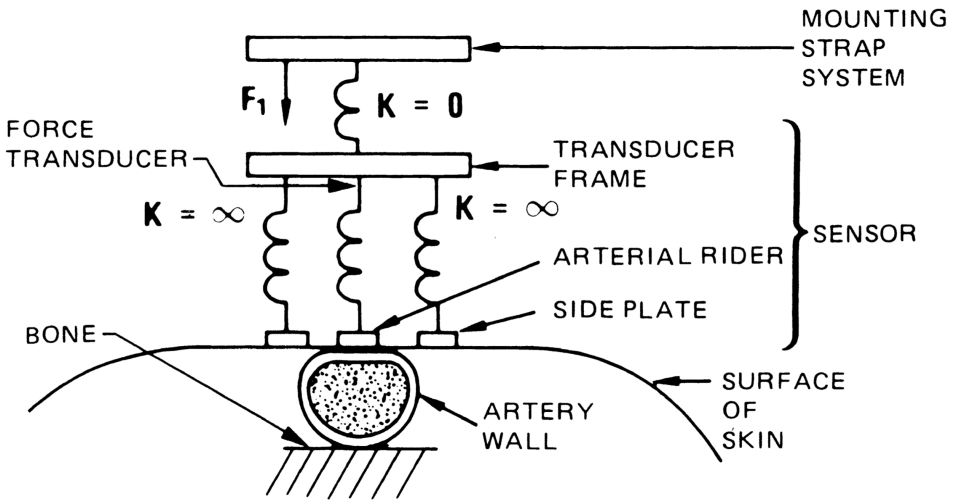

Figure 2.3: Schematic diagram of a tonometer sensor and a superficial artery [32]

This method has some important limitations, first, it measures peripheral pressure instead of more centrally-located pressures, this can lead to erroneous measurements in hypertensive patients with stiff arteries. Other disadvantages are:

- The sensitivity of the method to the sensor location;
- The need of calibration, the artery flattening degree depends on the hold down-force, and it is essential to a correct tonometric pressure measurement [32];
- Retail price is too high to be a standard method.

2.2 Electrocardiogram

The cardiac activity is closely linked to the creation and propagation of electrical action potentials. The electrocardiogram, or ECG, is a measure of the change in the heart electrical activity over time as the action potentials propagate in this same organ [35]. Due to the sequential depolarization and the contraction (which leads to movement) of the zone where the depolarization occurs, zones with opposite charges are created and can be analyzed as an electric dipole (Figure 2.4).

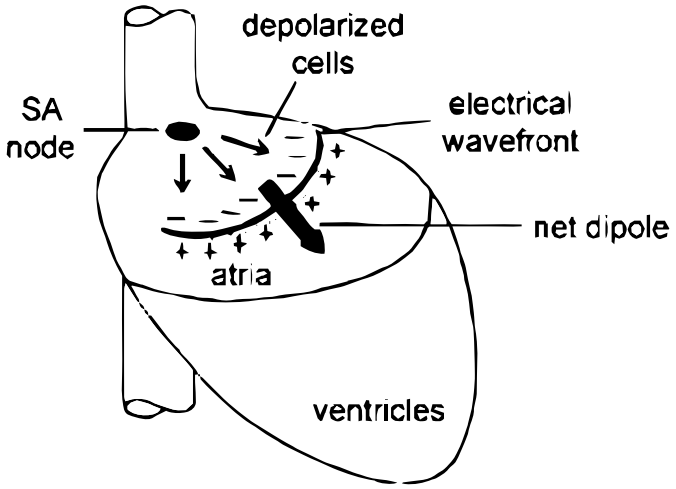

Figure 2.4: Hearth dipole formation [35]

The electric dipole formation in a conductive medium leads to an electric current creation that causes a change in the electric field. Changes that can be measured by placing electrodes on the surface of the body. The measured voltage depends on the electrode orientation in relation to the electric dipole at that point.

2.2.1 Electrocardiogram signal shape

The ECG signal is represented as a potential difference, usually in milivolts (mV), in order of time, usually represented in seconds (s). An example of the first lead (Lead I) ECG signal is shown in Figure 2.5.

The signal portion for each heart beat is easily identifiable (Figure 2.6)

The signal in the figure 2.6 results from the sum of the various action potentials that are created in various regions of the heart at different times. Because of that the ECG signal is a crucial medical factor in the cardiovascular system evaluation.

In a normal ECG signal it is possible to identify five characteristic points. The signal begins with a P wave (positive in leads I, II, and III) that results from the depolarization of the two atria, followed by the QRS complex (after an isoelectric segment or PR segment)

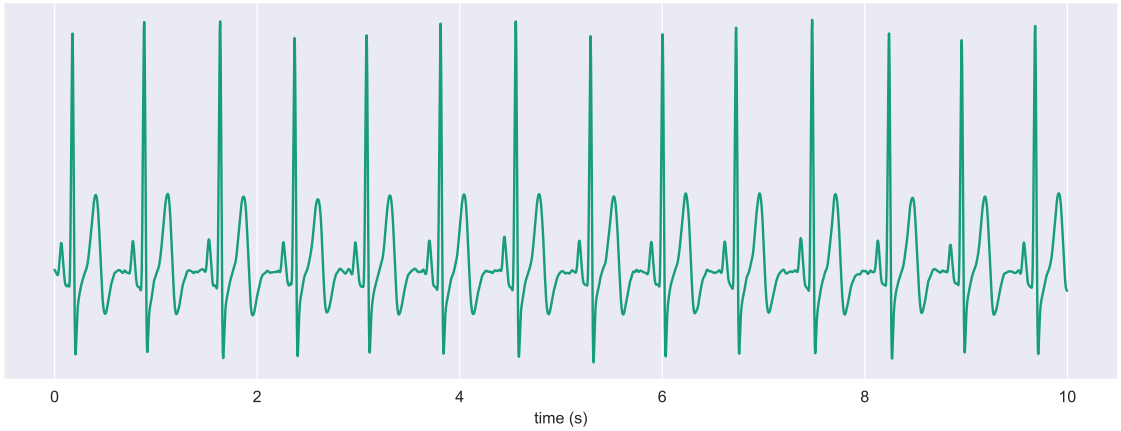

Figure 2.5: ECG segment

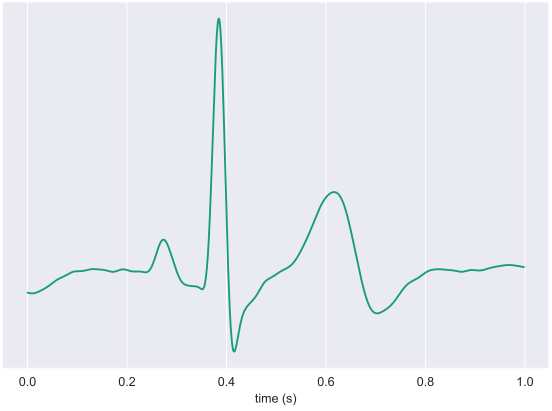

Figure 2.6: One ECG signal cycle

that results mainly from the ventricles depolarization and in a lower scale from the repolarization of both atria, and finally the T wave as a result of the ventricular repolarization. In some specific conditions a low amplitude wave can appear in the ECG signal (U wave).

Since the QRS complex is normally the most visually identifiable portion of ECG trace due to the bigger amplitude, it is usually used in the majority of the algorithms to identify each heart beat. As previously mentioned the QRS complex, more specifically the R peak, can be used as a proximal time reference point to calculate PTT.

2.2.2 Electrodes positioning

The electrodes positioning is a crucial factor in the obtained ECG signal since different electrodes position configurations result in slightly different signals. Figure 2.7 shows the standard electrode configuration for 12 leads (10 electrodes).

The use of several leads allows an analysis of the cardiac electrical dipole in different directions, both in the vertical plane (through the peripheral electrodes) and in the horizontal plane, through the precordial electrodes.

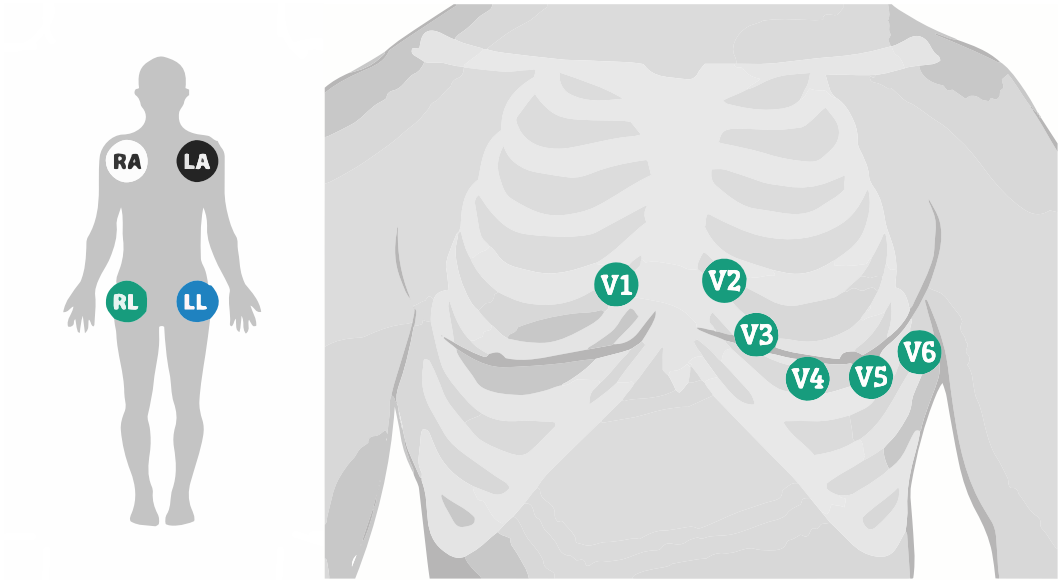

(a) Limb electrodes location (b) Precordial electrodes location

Figure 2.7: Electrodes standard locations, adapted from [36]

2.2.3 R Peak Detection Algorithm

Several algorithms to do an automatic detection of the R peak have been proposed throughout the years.

In 2002, Patrick Hamilton proposed and provided an open source algorithm do detect R peaks in the ECG signal [37]. The algorithm can be described in five different phases:

1. The signal is digital filtered with a low cutoff frequency of approximately 8 Hz and an high cutoff frequency of 16 Hz;
2. Differentiation and rectification of the signal;
3. Filter the signal with a 80 ms moving average filter;
4. Peaks detection;
5. Peaks correction.

The rules used to correct the detected peaks were defined empirically using physiologic limits the human body [37]:

- Ignore peaks that precede or follow larger peaks within 200 ms window;
- In the peak location check if the ECG signal has a positive and a negative slope. (To remove identified peaks that result from base line shifts);
- If the detected peak occurs in a 360 ms window after the previous peak and if the maximum slope is less than half when compared with the maximum slope of the previous peak, consider it a T wave peak;

- If the peak is larger than the detection threshold (adaptive threshold calculated based in estimates of the previous QRS peak and noise peak heights) is classified as a R peak, otherwise it is classified as a noise peak;
- If an interval equal to 1.5 times the mean RR interval has elapsed since the most recent detection, within that interval there was a peak that was larger than half the detection threshold, and the peak followed the preceding detection by at least 360 ms, classify that peak as a R peak.

The overall accuracy of this beat detector is close to 99.8% on the MIT/BIH and AHA arrhythmia databases [37].

2.3 Photoplethysmography

The PPG is a practical and straightforward optical method commonly used to detect changes in blood volume in the microvascular tissue bed [38].

2.3.1 Physical mechanism

The engineering underneath PPG is relatively simple, the device has a light source, that emits light into the tissue, and a photodetector, the receptor of light that interacted with that tissue. The photodetector can be placed adjacent to the light source in reflection mode PPG or in the opposite side (transmission mode PPG) [39]. Usually the light source depends on the objective, infrared light or near infrared light emitting diode are commonly used to measure blood flow that is more deeply concentrated in some parts of the body, and green light emitting diodes are usually used to calculate oxygen absorption in tissue, because radiation with that wavelength interacts differently with oxyhemoglobin and deoxyhemoglobin [40]. Another important point is the influence of light wavelength in PPG signal since penetration depth has a direct correlation with the wavelength of the light that is being used. As a consequence, light with a larger wavelength penetrates deeper in the skin (Figure 2.8) [39].

2.3.2 PPG waveform

The signal from PPG has two major components, an AC component, also called pulsatile, that comse from blood volume variation that arises from heartbeat, and a DC component (or almost DC), as a result of the presence of the tissue itself and from the average blood volume, this last component is influenced by respiration cycle, sympathetic nervous system and thermoregulatory processes [40], that causes low frequency changes in the signal.

As already said, the AC component of the PPG signal is caused by the heart activity and has a direct correlation with the heart's systolic and diastolic phase. That way, the PPG pulse can be divided into two portions, the first rising edge, between the valley and

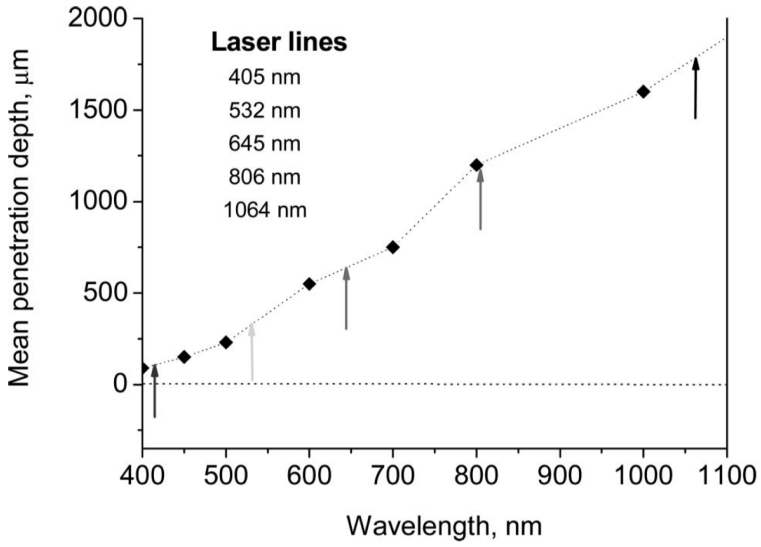

Figure 2.8: Mean penetration depth in order of light wavelength [41]

the pulse wave systolic peak, that represent systole, called anachrotic phase, and the next falling edge, also known as catacrotic phase, characterized by diastole. A notch (called dicrotic notch) could usually be identified in catacrotic phase because of the momentary increase in blood volume due to retrograde flow. (Figure 2.9) [42]. The temporal delay between the systolic peak and diastolic peak in the PPG signal, as well as the temporal position of the dicrotic notch are influenced by several factors, like the large artery stiffness, that normally is higher in older people [43]. Because of this factor the PPG waveform has slight differences between subjects.

2.4 Pulse Transit Time

The PTT is the time that the pressure wave created in the heart takes to travel between two different arteries sites. Several studies indicate that PTT is closely linked to BP values and can be used to estimate this physiological parameter due to vascular tone changes that result from variation in BP.

An acute rise in BP lead to an increase in vascular tone, the arterial wall becomes stiffer, lowering the pressure wave travel time (PTT). In the other hand, when the BP falls, the vascular tone decreases causing a rise in PTT.

Although it is not possible to directly correlate the absolute value of the PTT signal with absolute values of BP, it is possible to predict the variation of this parameter with PTT. This indicates that a process of calibration is usually needed when using PTT to estimate BP.

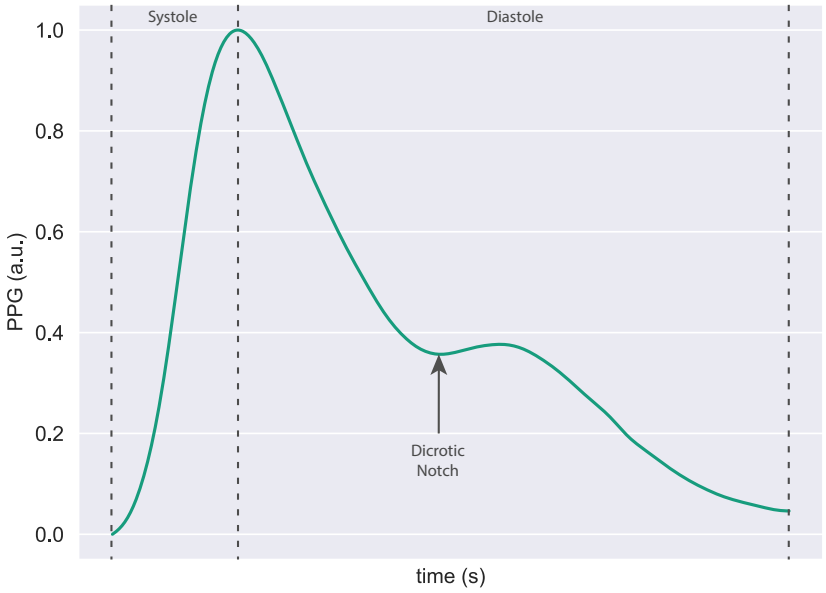

Figure 2.9: PPG signal cycle example

2.4.1 PTT calculation

Several methods can be used to calculate PTT, the most obvious is to use two PPG sensors in different positions, like finger and forearm or wrist and finger to detect the blood volume variation on both positions, the PTT is the time interval between correspondent positions in both signals. This approach is the most accurate among non invasive methods, but has some major disadvantages. Due to the PPG nature, this signal is very prone to motion artifacts that can lead to an impossible processing. Moreover, since the PPG needs to be acquired in positions with superficial blood vessels. The signals acquired in locations like arm and wrist have generally low signal to noise ratio or can not be detected in some cases.

To overcome this disadvantages it is usual to use the R peaks of the ECG as proximal time reference and finger PPG as distal time references to calculate the pulse arrival time (PAT). It is the sum of the pre-ejection period (PEP) (delay between the ventricular depolarization and the blood flowing from the heart) and PTT.

$$PAT = PEP + PTT \tag{2.2}$$

Several studies indicate that PAT can be used as a substitute of PTT in BP estimation with slightly worst results but with a setup that can be applied outside of the laboratory [44–46]. In most studies in this area, the term PTT is commonly used as synonym of PAT since use the setup ECG plus PPG lead to a much simple system to use in a day-to-day basis when compared with systems with two PPG or one PPG sensor and one microphone

in the chest (phonocardiogram).

Another important factor is the selection of the time point in the PPG signal to use as distal time reference for PTT. Three points are commonly used for this purpose, the onset point (systolic rising edge point where occurs the maximum variation) that leads to onset pulse transit time ($\mathbf{PTT_{onset}}$), the position of the maximum that leads to maximum pulse transit time ($\mathbf{PTT_{max}}$), and the PPG cycle beggining that leads to initial pulse transit time ($\mathbf{PTT_{init}}$).

2.4.2 Blood Pressure Relation

Most of the models that correlate BP and PTT come from Moens-Korteweg equation and Hughes equation or using empirical models.

The Moens-Korteweg equation [47] correlates the PWV with the vessel wall elastic modulus (Equation 2.3).

$$PWV = \sqrt{\frac{Eh}{2\rho r_i}} \tag{2.3}$$

Where E is the arterial wall Young's modulus, h is the wall thickness, ρ is the blood density, and r_i is the artery internal radius.

Hughes *et all.* recognised that the elastic modulus of the vessel increases exponentially with increasing blood pressure [48] (Equation 2.4).

$$E = E_0 e^{-\lambda P} \tag{2.4}$$

Where E is the elastic modulus of the wall, E_0 is the elastic modulus at zero pressure, P is the blood pressure and λ a coefficient that depends on the particular vessel.

Using equation 2.3 and equation 2.4 and knowing that PWV is inversely proportional to PTT

$$PWV \propto \frac{1}{PTT} \tag{2.5}$$

It is possible to conclude that [48],

$$P = -\frac{1}{\lambda}\log\frac{2k^2\rho r_i}{E_0 h} + \frac{1}{\lambda}\log PTT \tag{2.6}$$

Where k is a constant.

The equation 2.6 can be visually simplified replacing all constants with constant A and B. The final result is equation 2.7.

$$P = A + B \times \log PTT \tag{2.7}$$

On the other hand, knowing that [49]

$$\Delta P = E\frac{2\Delta r}{r_i} \tag{2.8}$$

And using equation 2.3 and 2.8 gives equation 2.9.

$$P = \frac{A}{PTT^2} + B \tag{2.9}$$

Where A and B are subject dependent constants, but different from equation 2.6 constants.

Several other models based in empirical observations have been used in this area, some of them using not only PTT but also other parameters like heart rate (HR). The table 2.2 resumes the physical models used in bibliography.

Table 2.2: Physical Models

Ref.	Model	HR use
[49]	$A \cdot PTT + B$	-
[50]	$\frac{A}{PTT^2} + B$	-
[51]	$A \cdot \log PTT + B$	-
[52, 53]	$\frac{A}{PTT} + B$	-
[54]	$A \cdot PTT^2 + B$	-
[54]	$A \cdot PTT^2 + B \cdot PTT + C$	-
[55]	$A \cdot PTT + B \cdot HR + C$	✓
[56]	$A \cdot \log PTT + B \cdot \log HR + C$	✓

2.5 Machine Learning

Machine learning and artificial intelligence are terms that, nowadays, can be found in several applications in science and even outside the lab environment in real functional applications.

Although, the terms Machine Learning and Artificial intelligence are commonly misused or misunderstood. As an example, knowledge graphs can be described as an artificial intelligence tool but are not machine learning. Therefore the machine learning systems/algorithms are a subset of artificial intelligence where the system can change itself when exposed to new data without the need of explicitly program changes or define any kind of rules [57].

2.5.1 Types

Machine learning techniques can be classified in different categories based on some characteristics [57, 58]:

- **Supervised Learning:** in this category of machine learning methods, the model is fed with a group of input sets (X) and the correspondent output (Y). The objective

is to get the mapping function M (or usually an approximation) that correlates the input variables with the given outputs.

$$Y = M(X) \tag{2.10}$$

It can be further divided in two categories, classification models, when the output variable is categorical, for example "Grade 1 hypertension", "Grade 2 hypertension", "Normal BP", and so on, and regression models, when the output is a continuous variable itself, like the BP value.

- **Unsupervised Learning:** Unlike supervised learning, in this category of machine learning approaches only the set of features are given to the model, usually because the labels are not available, with the aim of divide a data set into clusters, considering their similarities.
- **Semi-Supervised Learning:** It is a mix between supervised and unsupervised learning where part of the data is unlabeled.

  With this approach, the labeled and unlabeled data can be fed into an clustering system (unsupervised learning) that label the non-labeled data based on similarities, and then use the resultant data to make predictions of new data (supervised learning).
- **Reinforcement Learning:** In this machine learning category trial and error approaches are used to find a solution to a specific problem. The solver performs a random action and gets rewards if the result contributes to attain the final objective or penalties if the opposite happens.

In this work the focus will be supervised learning regression methods and in some specific points unsupervised learning methods, since the objective is to predict BP values, that is a continuous variable, based on past observations, that are used to train the model.

2.5.2 Algorithms

The regression algorithms will be discussed in this section, they can be as simple as a linear regression model or more complex as neural network (NN). There are no master key model for all problems, the pros and cons of each model should be evaluated and outcome should be used to define the best model.

2.5.2.1 Linear Regression

The linear regression is the simplest form of regression, the objective is to model a given training data with a linear function. This way the predicted value results from a linear combination of the features (equation 2.11).

$$\hat{y}(\omega, x) = \omega_0 + \omega_1 x_1 + \omega_2 x_2 + ... + \omega_n x_n \tag{2.11}$$

Where $\hat{y}$ is the predicted value, $x = (x_0, x_1, x_1, ..., x_n)$ comprises the computed features, $\omega = (\omega_1, \omega_2, ..., \omega_n)$ is the coefficients vector, and ω_0 is a intercept value.

The objective is to find ω and ω_0 that better fits the training data and then make predictions with each new x. The process of finding the best ω can be achieved based on cost function J minimization, like ordinary least squares [59].

$$min(J(\hat{Y}, Y)) = min(\frac{1}{n}\sum_{i=1}^{n}(\hat{y} - y)^2) \tag{2.12}$$

2.5.2.2 Random Forest

The random forest (RF) is an ensemble approach for classification or regression. An ensemble learning method uses several prediction algorithms with the goal of improving the overall accuracy of system [59]. In this case, as can be interpreted by the name, a RF learning method uses decision trees as fundamental structures, thus the decision tree learning algorithm will be briefly explained in the following paragraphs.

A decision tree is a simple algorithm inspired in the human decision process, and due to this fact it is usually well understood by users in contrast with black-box algorithms like NN [59]. The tree is normally constructed from top to bottom where each node represents a feature, the process can be simplified in some steps:

1. Train data selection;
2. Best feature selection;
3. Split the data according with the possible values of the selected feature (node creation);
4. Recursively repeat points 2 and 3 with the subset of data that results from the last point;
5. Stop when stopping criteria is reached.

It is important to explain some of the points above, the feature selection can be processed using several criteria, like impurity based, gain ratio, distance measure, among others. But the core objective is to select the feature that better describes the problem (figure 2.10). The growth of the tree should also be controlled since a bigger tree is more prone to suffer from overfitting and takes longer to be trained, several conditions can be used like the tree maximum depth and maximum leaf nodes. An additional step of pruning can be made so that unnecessary splits are removed, this process simplifies the tree and leads to a sub-tree that is less affected by overfitting in the train data.

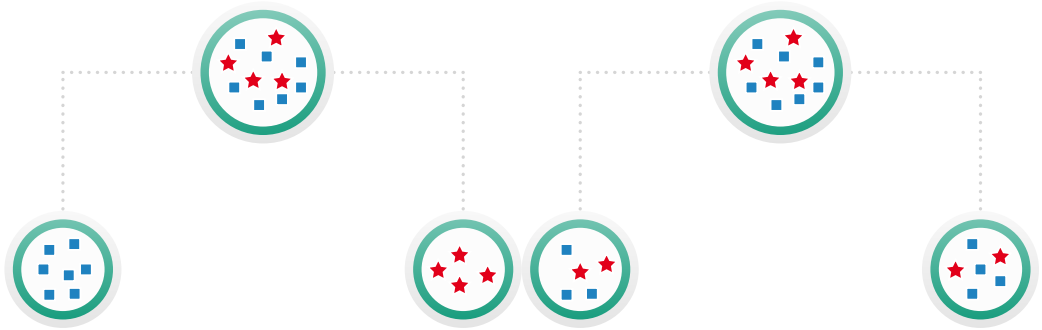

(a) High information gain (b) Low information gain

Figure 2.10: Difference in information gain based on the feature selected, it is the amount of information that is gained by knowing the value of the attribute, which is the entropy of the distribution before the split minus the entropy of the distribution after it. The largest information gain is equivalent to the smallest entropy.

Although, trees generally do not have the same level of accuracy as some of the other regression and classification methods. As a solution, the predictive performance of trees can be substantially improved using random forests [59].

The improvement can be explained using statistical concepts [60]. Given a set of n independent observations $F = \{F_1, F_2, ..., F_n\}$, each one with variance σ^2, the variance of the mean of the observations is equal to the mean of the variances.

$$V(\bar{F}) = \frac{1}{n}\sum_{i=1}^{n} V(F_i) = \frac{\sigma^2}{n} \tag{2.13}$$

The only adaptation that is necessary is to bootstrap (taking repeated samples from the training data set) since only one training data set is available. This way, using RF, several decision trees are created, but in contrast with Bagging method, where the trees are created choosing the best feature in each node from all features, the chosen feature is selected from a group of a certain number of randomly selected features. This change improves the decorrelation between trees.

2.5.2.3 Neural Network

The work and investigation with NN results from the understanding of how human brain works when transforming a complex group of inputs into a simple action or output. This way, just like the human brain, an artificial NN is a massively parallel distributed processor, capable of storing experimental knowledge and making it available for feature use [61]. It consists of several elementary units, called neurons.

A model of a digital neuron based on the McCulloch-Pitts model [62] is represented in figure 2.12, as well as the tree neuron main components:

- A set of synapses that are characterized by synaptic weights, $\omega_{k1}, \omega_{k1}, ..., \omega_{km}$, that can be seen as the importance of that input to the overall neuron output;

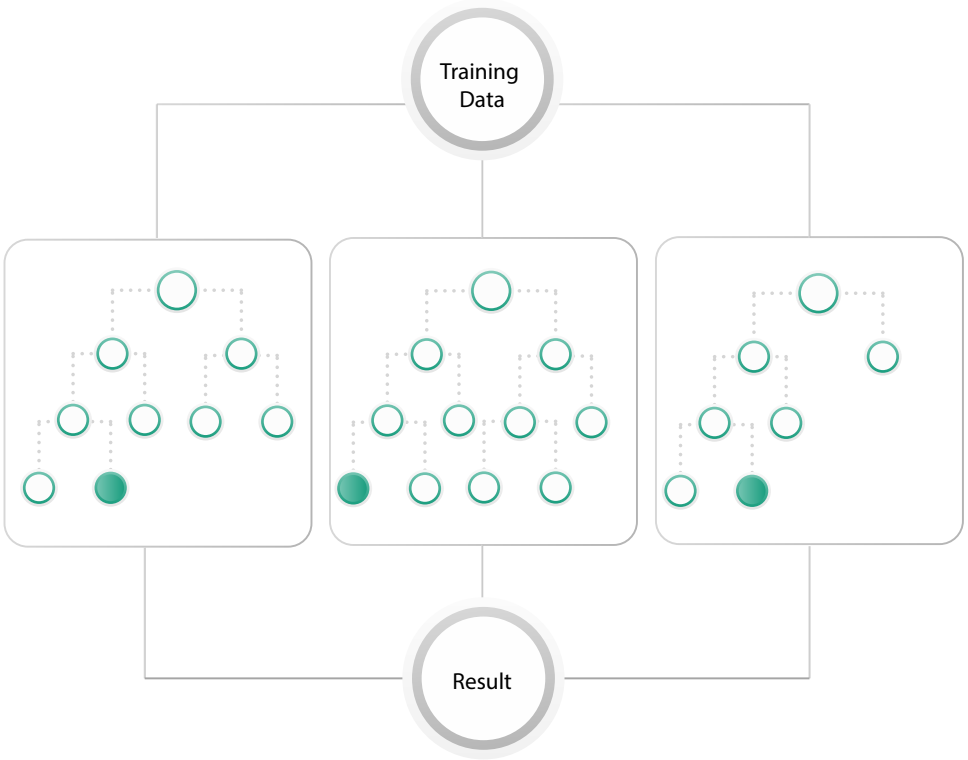

Figure 2.11: Random Forest method representation, it operates by constructing a multitude of decision trees at training time and outputting the class that is the mode of the classes (classification) or mean prediction (regression) of the individual trees.

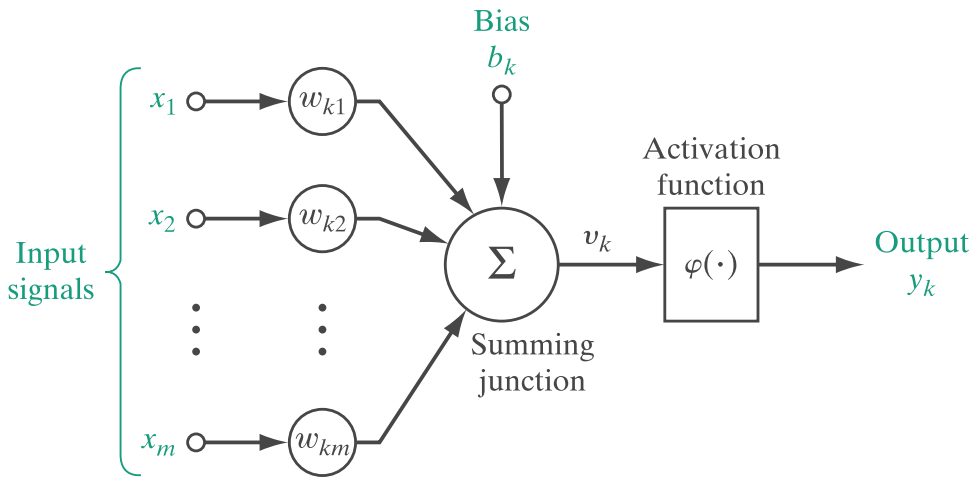

Figure 2.12: Artificial neuron representation, adapted from [61]

- A adder function, that adds all input signals weighted by the respective synaptic strengths;
- And an activation function to limit the amplitude of the neuron output.

It is common to include a bias input to increase or decrease the net input of the activation function, this helps controlling the activation function [61, 62], allowing to shift it in the horizontal axis. Usually it is represented as a fixed input of value 1 with a specific weight equal to the bias. The neuron can be mathematically explained in the following equations:

$$v_k = \sum_{j=1}^{m} \omega_{kj} x_j + b_k \tag{2.14}$$

$$y_k = \phi(v_k) \tag{2.15}$$

Where $x_1, x_2, ..., x_m$ are the inputs, $\omega_{k1}, \omega_{k2}, ..., \omega_{km}$ are the respective weights, b_k is the bias and ϕ the activation function.

As mentioned previously, an artificial NN, or commonly just NN, is a combination of simple neuron units, typically grouped in layers. In figure 2.13 is represented a feed-forward multi-layer network, where each output of a layer of neurons is fed as input to each neuron of the next layer, in this network tree different layers can be identified, a input label that receives the input data, one or more hidden layers where the core of the computation occurs, and an output layer that converts the activation result in the hidden layer to an output that can be the class (when the problem is a classification) or a value (when the output is the result of a regression problem). There are other types of networks like Radial Basis Functions NN, Recurrent NN, among others, but the scope of this dissertation will be only the simplest case of NN.

Before it is possible to use a NN to make predictions, it is necessary to train it first. The training is generally performed giving to the network several examples of inputs for which the outputs are known, and update the weights using the errors.

A common algorithm to perform this training iteratively is the back-propagation algorithm. It can be simplified in some steps [61, 63]:

1. **Model initialization:** The weights are randomly initialized;
2. **Foward propagation:** Then the input vector is propagated forward through the NN;
3. **Loss function:** The output values are then compared with the real known values, this comparison is performed using the chosen loss function, for example, the absolute difference between the calculated values and the real values or more frequently the sum of squares of the absolute errors;
4. **Differentiation:** Computation of the loss function gradient, since it gives the rate with which the function is changing;

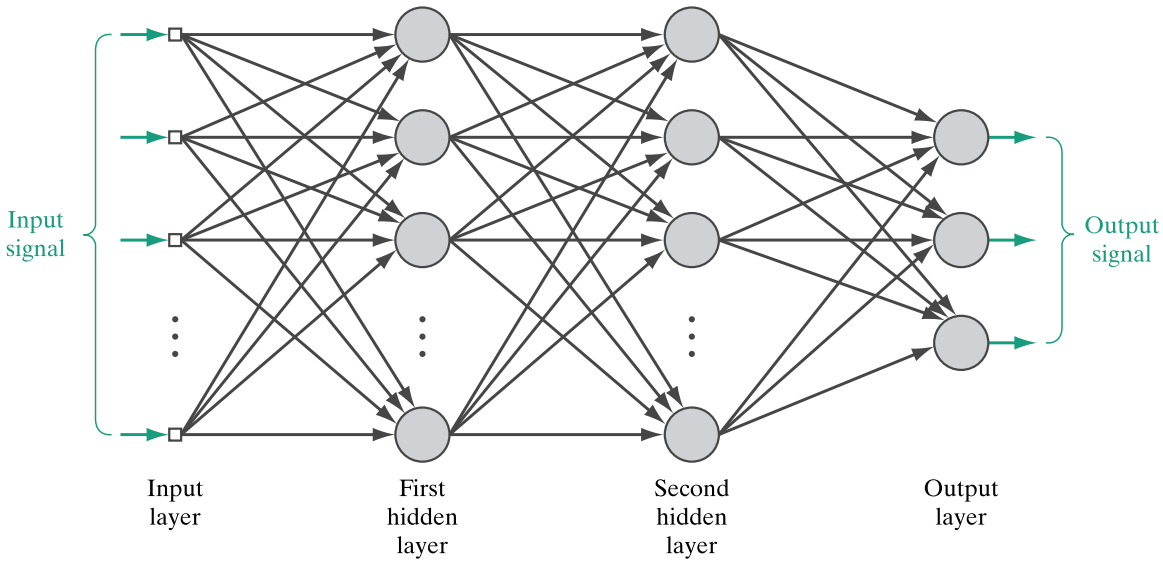

Figure 2.13: Fully-connected multi-layer neural network representation, adapted from [61]

5. **Back propagation of the error:** The error values are then propagated backwards through the network to calculate the error values of the hidden layer neurons. The loss function gradients of the hidden neurons can be solved using the chain rule;

6. **Weights update:** The weights are updated using the delta rule [64], defined by:

$$\Delta\omega_{ji} = \alpha(y_j^* - y_j)\phi'(h_j)x_i \tag{2.16}$$

   Where α is a constant (learning rate), ϕ is the neuron's activation function, y_j^* is the target output, h_j is the weighted sum of the neuron's inputs, y_j the output, and $\omega_i j$ is the ith input.

7. **Iterate:** This procedure is repeated until the weights converge.

2.5.2.4 Adaptive Boosting

The adaptive boosting (AdaBoost) is a machine learning algorithm first developed by Yoav Freund and Robert Schapire. Just like RF, boosting is an approach based on the idea that several relatively weak and inaccurate rules combined can lead to an highly accurate prediction rule [59]. The main difference is that the objective here is to create sequential weak predictors, so that the following predictor uses information from the present predictor. Adaboost can be resumed in the following points [59]:

1. Adaboost combine multiple weak predictors;

2. The weak predictors are sequentially generated.

3. The instances selected from the training set are not randomly selected, instead they are chosen based on the relative weights that are updated in each iteration

(instances that are missclassified have a greater probability of being selected in the next weak predictor);

4. Each weak predictor is associated to a constant α that is calculated based on how good that predictor is.

The final result of the predictor is given by equation 2.17

$$H(x) = \sum_{i=1}^{I} \alpha_i h_i(x) \tag{2.17}$$

Where H is the final hypothesis, α_i is the assigned weight associated to the ith weak predictor h_i.

2.5.2.5 Principal Component Analysis

The principal component analysis (PCA) is usually used to reduce the dimensionality of data sets preserving the most information. This reduction in the number of features can be used to help visualizing the data, for example when five features are reduced to three features, these can be plotted and visually analyzed. This method can also be used to reduce the total number of features used in the training process, so that the computational needs and training time are reduced.

2.5.3 Evaluation

A crucial characteristic of a machine learning model is how well the model can generalize to new unseen data. When a trained model cannot deliver the best results when evaluating new data it is possible that the model is overfitted to the training data.

To evaluate this scenario it is common to divide the data set in two or three groups:

- **Training set:** The data that will be used to train the machine learning model;
- **Validation set:** An 'optional' set that can be used to fine tune the model hyperparameters (parameters set before the learning process) with new unseen data;
- **Test set:** A set of unseen examples used only to assess the performance of the model.

One important factor when evaluating a model is to choose a test data set that is representative of the data set as a whole and sufficiently large to yield statistically significant results.

Several metrics can be used to perform the model evaluation, since this work focus on regression problems, the usual metrics to evaluate the models are:

Were n is the number of samples, y the real value and y^* the estimated value.

- **mean error (ME)**

$$ME = \frac{1}{n}\sum_{i=1}^{n} y - y^* \tag{2.18}$$

- **mean absolute error (MAE)**

$$MAE = \frac{1}{n}\sum_{i=1}^{n} |y - y^*| \tag{2.19}$$

- **root mean squared error (RMSE):** Sensitive to larger errors

$$RMSE = \sqrt{\frac{1}{n}\sum_{i=1}^{n} (y - y^*)^2} \tag{2.20}$$

- **Coefficient of Determinations (R squared):** provides indication of how good is the fit between predictions and actual values.

$$R^2 = 1 - \frac{SS_{res}}{SS_{tot}} \tag{2.21}$$

  Where $SS_{tot} = \sum_i (y_i - \bar{y}^2)$, $SS_{res} = \sum_i (y_i - \hat{y_i})^2$, y_i is the measured value, $\hat{y_i}$ the estimated value, and $\bar{y}$ the mean value of y.

2.6 Time Series Analysis

The time series analysis domain comprise methods to analyze time series data (set of observations x_t, measured over time t) in order to extract useful information and statistics from that data.

Time series analysis can be divided in several areas, in the context of this work the objective will be to measure the similarities between two time defined signals.

2.6.1 Pearson Correlation Coefficient

Although Pearson correlation coefficient is not a specific time series analysis tool, it can be used to calculate the correlation between two different variables.

It can be calculated with equation 2.22

$$r = \frac{\sum_{i=1}^{n}(x_i - \bar{x})(y_i - \bar{y})}{\sqrt{\sum_{i=1}^{n}(x_i - \bar{x})^2}\sqrt{\sum_{i=1}^{n}(y_i - \bar{y})^2}} \tag{2.22}$$

Where n is sample size, x_i and y_i are the individual sample points of each variable indexed with i, $\bar{x}$ and $\bar{y}$ are the mean of each variable. This coefficient vary between -1 and 1, where 1 is total positive linear correlation, -1 is total negative linear correlation and 0 is no linear correlation.

2.6.2 Dynamic Time Warping

The dynamic time warping (DTW) is a algorithm used to measure the similarity between two temporal sequences $A = a_1, a_2, ..., a_n$ and $B = b_1, b_2, ..., b_m$ that can vary in speed, and works calculating the distance between all points of both series. This results in a $n \times m$ matrix D where each position is given by $D_{ij} = distance(n_i, m_j)$, with $i \in \{0, 1, ..., n\} \wedge j \in \{0, 1, ..., m\}$, and then find the optimal path from $(0, 0)$ to (n, m), minimising cumulative distance of the path.

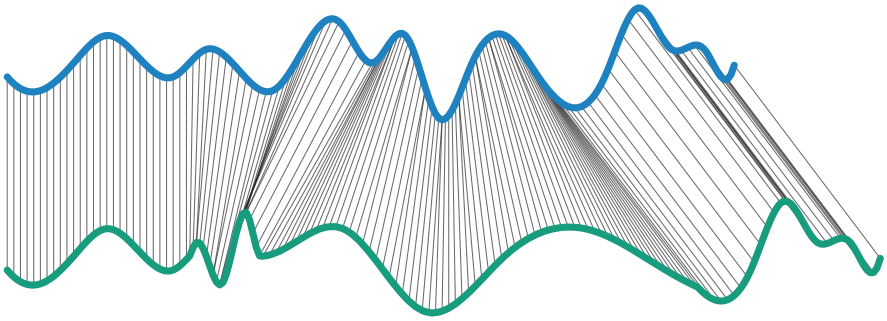

Figure 2.14: DTW representation, adapted from [65], the signals have the same characteristics, but with different velocities

Chapter 3

Blood Pressure Estimation With biophysical Models

This chapter contains the majority of the information about the materials used to estimate BP using the biophysical models presented in chapter 2 as well as a complete description of the methodology.

3.1 State of the Art

In 1981, Gueddes *et al.* [66] conducted a laboratory experiment in 10 anesthetized dogs, with the objective of evaluate the relationship between PAT and BP. Two different methods were used, to calculate PAT, the first one using the signal from two pressure transducers in different arterial points (in carotid and femoral arteries), and the second one using ECG and carotid pressure signal. The BP was raised with epinephrine injected intravenously and lowered with vagal stimulation. The results indicate that the PWV calculated with PAT increase nearly linearly with BP.

In 2000, Chen *et al.* [49] proposed a method to estimate BP using PAT and intermittent re-calibration with 5 minutes period. The BP was estimated by combining two acquired components, a low frequency component from the intermittent measured BP, and a high frequency component, that represents the variation of BP between intermittent BP measurements. This component was obtained by extracting a specific frequency band from PAT signal. The PAT was determined using the R peak in ECG and the onset of fingertip PPG sensor, the intra arterial BP was used as reference in both calibration and test. The study was performed in 20 subjects during cardiovascular surgery. The mean correlation coefficients between estimated and reference BP was 0.97 with standard deviation (SD) of 0.02, the RMSE mean value was (3.70 ± 1.85)%, and the mean error was (0.06 ± 0.68)%.

In 2005, Poon and Zhang [67] developed a cuffless and noninvasive technique for measuring BP using PAT (denominated as PTT in the article) based on Moens-Korteweg's formula. The data acquisition was performed in 85 subjects (39 hypertensives, 9 with congestive heart failure and 13 suffering from diabetes mellitus, 37 were healthy subjects), the protocol consisted in recording ECG, PPG and BP using a conventional mercury sphygmomanometer, first for calibration procedures and, after that, a set of measures was performed to evaluate the system. After a period of 1 month the test was repeated. This approach concluded that PTT-based approach can estimate SBP and DBP within 0.6 ± 9.8 mmHg and 0.9 ± 5.6 mmHg of the reference measurement, respectively.

In 2009, Chen *et al.* [47] proposed a new mathematical model that relates PWV and BP. Two PPG (toe and and earlobe) were used to calculate beat-to-beat PTT values, the BP values were acquired invasively with a pressure transducer inside the radial artery. In order to avoid individual calibration for each subject, the calibration was performed for groups of subjects, creating benchmark models for different groups, based on age and gender. The calibration benchmarks were created using data from 23 subjects, while the clinical verification of the models was performed in 20 different subjects. The results of this approach have met the AAMI test standard for DBP, with absolute mean deviation of 1.4 mmHg and SD of 7.5 mmHg, outperforming the auscultatory method. This approach is only suitable for people who do not have cardiovascular problems, in these cases an individual calibration process is still necessary.

In 2016, Ding *et al.* [7] proposed a model that uses not only PTT, but also a new indicator called photoplethysmogram intensity ratio (PIR), that can be affected by changes in the arterial diameter, therefore it can be used to track low frequency changes in BP. The algorithm was evaluated in 27 healthy subjects using the BP data from Finapress as reference. The proposed model had a MAE of 4.09 mmHg and 3.18 mmHg of SBP and DBP respectively .

In 2017, Carek *et al.* [68] developed a watch type device denominated SeismoWatch, including a PPG sensor (used as distal time reference) and an accelerometer to measure the thoracic vibrations that mark the heart contraction (proximal time reference). The device was tested with 13 healthy young subjects, with no history cardiovascular problems. The acquisition protocol was divided in three phases, first, the subject performed a series of exercises to vary the BP (used in calibration), second, the system was evaluated one day after calibration, and finally where a multiple-day test was performed. The group RMSE was 2.9 mmHg and 4.8 mmHg for DBP and SBP, respectively.

The aim of this chapter is to evaluate different models proposed in several papers based in the same metrics and data, as well as test the influence of different devices in the overall accuracy of the system. This represents an important step for future investigations, since it is impossible to compare previous works between them due to different evaluation metrics, and protocols.

3.2 Materials and Methods

3.2.1 Subjects

The subjects characteristics can be found in table 3.1.They were recruited based on convenience sampling, and only the subjects capable of performing the requested isometric leg exercise, were enrolled for the study. None of the subjects underwent cardiovascular surgery and only one of the 20 selected subjects was previously diagnosed with hypertension (stage 2) and was taking medication at the time to lower the BP (Enalapril 20 mg once a day). From the 20 subjects and based only on the acquired data in this study, 11 subjects were classified as having normal BP values, 6 as pre-hypertensive, and 2 as hypertensive stage 1.

Table 3.1: Subjects characteristics

Number of Subjects	20
Gender (M/F)	9/11
Age (Mean ± SD)	(29.75 ± 12.17) years
Maximum Age	62 years
Minimum Age	18 years
SBP (Mean [Min;Max])	(123.16 [96;152]) mmHg
DBP (Mean [Min;Max])	(79.69 [64;90]) mmHg

3.2.2 Acquisition Device

Two different devices were used to acquire both ECG and PPG signals, a description of those devices can be found in table 3.2. The BP values were acquired using an oscillometric automatic device from A&D (UA-651BLE), the full protocol of acquisition can be found in annex A.

Table 3.2: ECG and PPG acquisition devices

	Device A	**Device B**
Device	Biosignalsplux	Bitalino
Sampling Rate	1000 Hz (capable up to 3000 Hz)	1000 Hz
Resolution	16-bit	10-bit
ECG sensor	Gain: 1100	Gain: 1000
PPG sensor	Gain: 34 Wavelength: 670 nm Transmittance	Gain: - Wavelength: 565 nm Reflective

3.2.3 Data Collection Procedure

Data were collected following a standard protocol at Fraunhofer AICOS offices in Lisbon and at *Postura Ímpar* clinic.

The protocol comprises four stages, resulting in four distinct datasets for each subject:

- **Calibration set:** This dataset includes continuous PPG and ECG signals and sequential BP measurements. During the first five BP measurements the subjects were in rest, and the following while performing a leg extension exercise that was maintained until reaching muscular fatigue. This exercise leads to a rise in BP [69];
- **Static Test set:** This set contains three BP measurements with the respective continuous ECG and PPG signals acquired in static mode, without inducing variation in BP;
- **Dynamic Test set:** This set contains three BP measurements with the respective continuous ECG and PPG signals acquired while subject is performing a leg extension exercise that leads to a rise in BP;
- **Follow-up Test set:** This set corresponds to a repetition of the Static Test Set and Dynamic Test Set after not less than one week nor more than two weeks following the calibration and initial measurements of each subject. It contains six BP measurements with the respective continuous ECG and PPG signals.

Due to subject unavailability, the Follow-up Test Set was not collected for three of the subjects.

3.2.4 Pre-processing and PTT Calculation

Figure 3.1 depicts examples of the ECG and PPG signals acquired with device B. Two main issues that need pre-processing correction can be identified: the high frequency noise in the ECG signal, and the PPG signal saturation that mostly happens in device B.

To overcome these issues, a pre-processing phase is necessary to guarantee a good signal quality and minimise errors in subsequent processing steps. The ECG signal is filtered in both directions, to remove phase shift, using a digital bandpass finite impulse response (FIR) filter with low frequency of 0.5 Hz and high frequency of 30 Hz. In PPG signal, an additional step to interpolate the signal in the saturation zone is performed, first the saturation zones are detected based on the value of the signal and the respective analog to digital converter (ADC) maximum value, then it is interpolated using cubic spline interpolation and the information in a window of 100 ms before and after the saturation zone. The signal is then filtered in both directions using a digital band-pass FIR filter with low frequency of 0.5 Hz and high frequency of 3 Hz to remove high frequency noise.

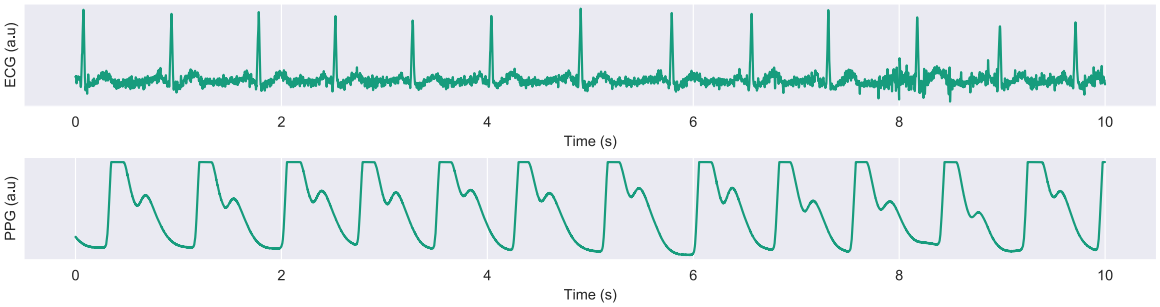

Figure 3.1: Raw signals

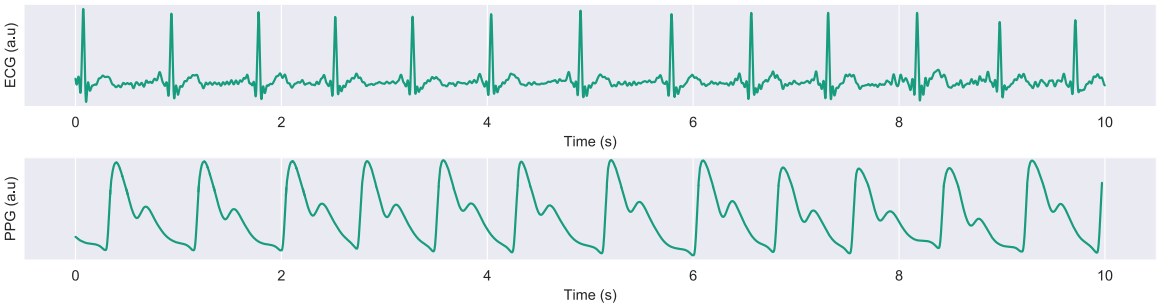

Figure 3.2: Pre-processed signals

Several works from different authors indicate that the PTT, defined as the time that the blood takes to travel between two different arteries points, is highly correlates with the BP. Therefore, the PTT has the potential to be used as BP tracker. As mentioned in chapter 2, in this work, the R peaks of the ECG signal are used as proximal time references, and three different points, Figure 3.3 (cycle maximum, start and onset), from PPG signal are tested as distal time references with the objective of assessing which one leads to better results.

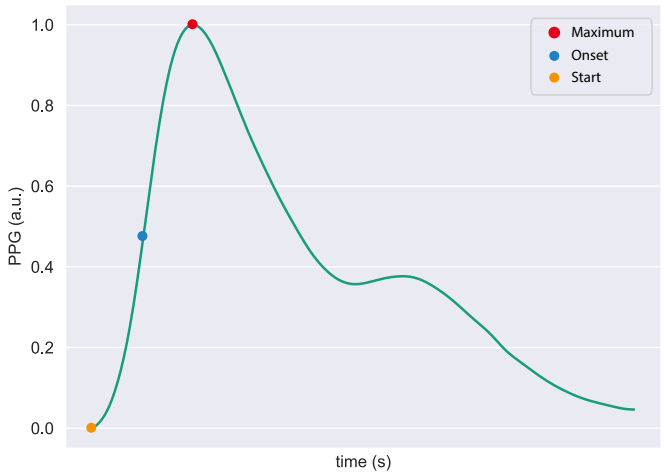

Figure 3.3: Example of PPG points tested as distal time references in PTT calculation

Hence, the first step to calculate the PTT signal is to identify the proximal and distal points in ECG and PPG signals, respectively. The R peaks in the ECG signal are identified using the algorithm proposed by Hamilton, described in chapter 2 and implemented in BioSPPy toolbox [70]. An example of he result of the application of this algorithm can be found in figure 3.4.

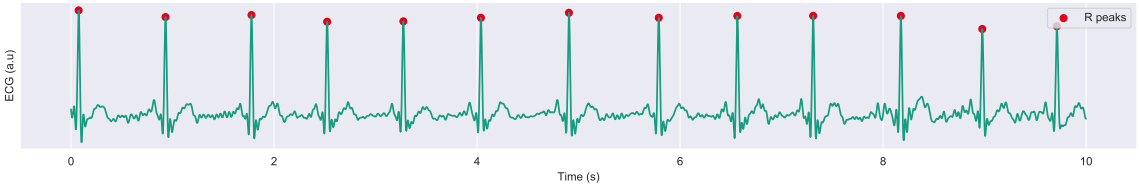

Figure 3.4: Example of the detection of R peaks in an ECG signal using Hamilton R peak detection algorithm. Green line: EEG signal, red dots: R peaks detected.

The process identification of the three fiducial points in the PPG signal begins with the identification of the maximum in each cardiac cycle. The process of identifying the maximum of the PPG in each cardiac cycle can be decomposed in two different phases:

1. **Adaptive peak detection:** This phase is based on the approach present in HeartPy module [71]. First, the rolling mean of the PPG signal with a 0.75 seconds window is calculated. Then, the peaks are identified as the maximum of each portion of the PPG signal above the rolling mean signal, from the peak location it is possible to calculate the RR standard deviation (RRSD), and the mean cardiac frequency.

   This procedure is repeated several times with different vertical shifted signals based on the rolling mean signal. The final result are the peaks that result in the lower non-zero value of RRSD and have cardiac frequency between 40 beats per minute (BPM) and 180 BPM, used in this stage as physiological limits at rest.

2. **Correction:** The previous phase is usually enough for a correct identification of most peaks, although, in very specific situations some errors may occur. To overcome these errors and get a more robust algorithm the ECG signal is used as a correction tool. If more than one PPG peak is detected between two consecutive R peaks in the ECG signal, the peak with the highest amplitude is considered the systolic peak (maximum), and it is used for PTT calculation. This is especially useful when the first part of the algorithm erroneously detects both systolic and diastolic peaks, instead of only systolic peak as it was supposed to.

The other two fiducial points from PPG signal, cycle start and onset, are calculated relatively to the maximum of the PPG signal, previously identified for each cardiac cycle. The cycle start is defined as time value corresponding to the minimum of the signal between two consecutive PPG maxima, and the onset point is defined as the time value with greater gradient between the cycle start and the maximum of the PPG.

The PTT is calculated subtracting the proximal and distal time references of the same cardiac cycle (equations 3.1, 3.2, 3.3). The PTT is considered valid if it falls within the range $[0.2 \times RR; 0.7 \times RR]$

$$PTT_{init} = t_{init} - t_{rpeak} \tag{3.1}$$

$$PTT_{max} = t_{max} - t_{rpeak} \tag{3.2}$$

$$PTT_{onset} = t_{onset} - t_{rpeak} \tag{3.3}$$

Where t_{rpeak} is the ECG R peak location (in time) and the t_{init}, t_{max}, t_{onset} are the location in time of the initial, maximum and onset points on the correspondent PPG cycle.

An example of the resultant PTT signal can be seen in figure 3.5, in some cases, due to R peaks misidentification, spurious peaks can be identified in PTT signal. These can be corrected by performing a median filter with a window size of 3 samples. The resultant signal of this procedure is represented in figure 3.6.

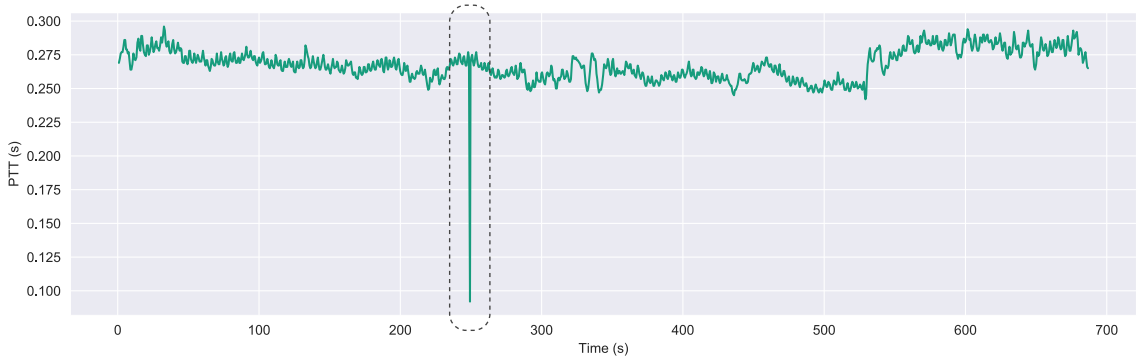

Figure 3.5: PTT signal pre median filtering

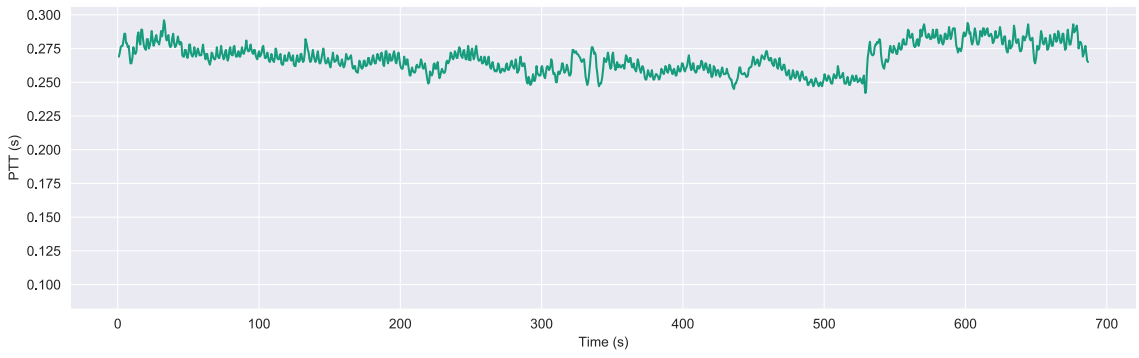

Figure 3.6: PTT signal post median filtering

3.2.5 Blood Pressure Estimation

As presented in chapter 2 several biophysical models have been proposed to predict BP from PTT. The main difference between the approach taken in this work and bibliography described in the beginning of this chapter is that the calibration procedure is usually performed using expensive BP meters that give continuous measurements, like the Finometer, and in this work the calibration is performed using an automatic device that can be easily used at home.

The models tested in this work were selected from previous works based on their reported performance, the models with higher performance are compiled in table 3.3.

Table 3.3: Biophysical models used in this work, where A, B and C are subject and model dependent constants

Model	Equation
(1)	$BP = A \cdot PTT + B$
(2)	$BP = A \cdot \log PTT + B$
(3)	$BP = \frac{A}{PTT} + B$
(4)	$BP = A \cdot PTT^2 + B$
(5)	$BP = A \cdot PTT^2 + B \cdot PTT + C$
(6)	$BP = A \cdot PTT + B \cdot HR + C$
(7)	$BP = A \cdot \log PTT + B \cdot \log HR + C$

The calibration needs to be performed for each subject. Since the cuff-based BP measurement does not reflect an instantaneous value of the BP, but rather the BP in a window of time, the PTT values used for calibration are the mean of the PTT signal in a window of ten seconds before the BP measurement (figure 3.7).

The pairs (BP, PTT) (or in case of the models that use HR, the triplets (BP, PTT, HR) are then used to calculate the constants of each model for each subject. This procedure is performed using ordinary least squares algorithm implemented in scikit-learn [58] for each SBP and DBP value. In Figure 3.8 is an calibration example from the signal present in Figure 3.7.

After the constants determination it is possible to estimate the BP values referent to the new PTT values.

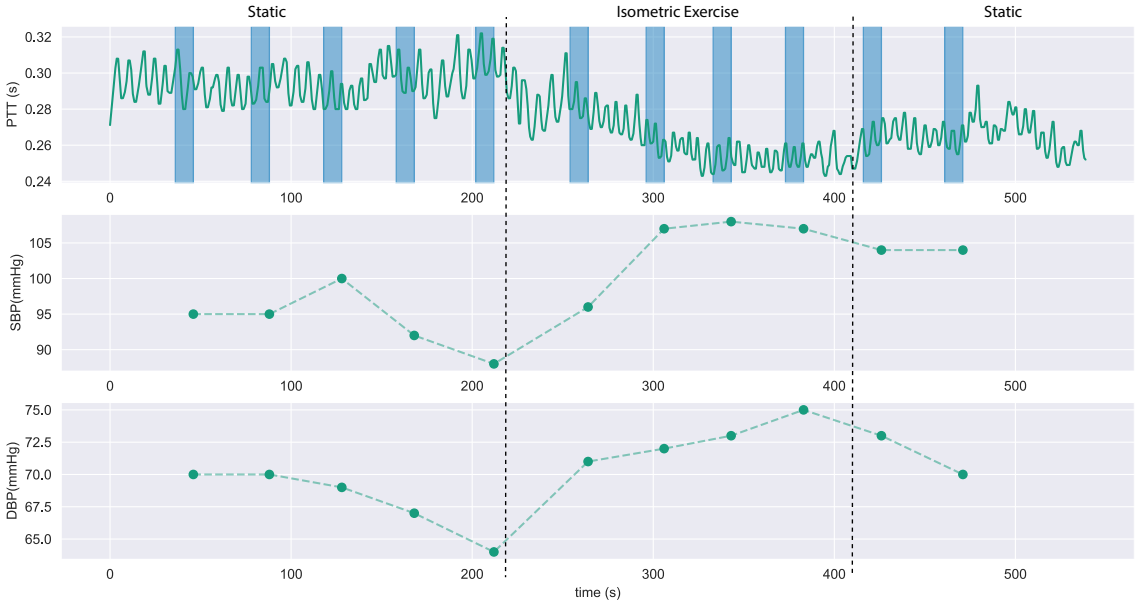

Figure 3.7: Subject 09 PTT and BP calibration signals

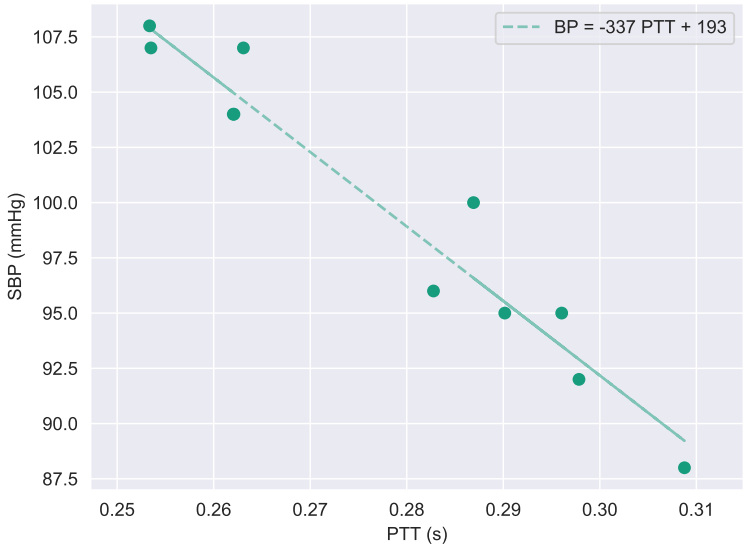

Figure 3.8: Subject 09 linear model calibration example

3.3 Results

3.3.1 Calibration

The calibration process was performed for each SBP and DBP values. With the objective of understanding which distal reference point of the PPG cycle led to better results, the calibration procedure was also performed with the different PTT values ($\mathbf{PTT_{init}}$, $\mathbf{PTT_{onset}}$, $\mathbf{PTT_{max}}$). The results can be observed in Table 3.4.

Table 3.4: All subjects coefficient of determination mean and SD correspondent to SBP and DBP calibration (Device A)

Model	Measure	$\mathbf{PTT_{max}}$		$\mathbf{PTT_{onset}}$		$\mathbf{PTT_{init}}$	
		$\overline{R^2}$	SD	$\overline{R^2}$	SD	$\overline{R^2}$	SD
(1)	SBP	0.77	0.16	0.81	0.11	0.40	0.29
	DBP	0.72	0.17	0.75	0.14	0.36	0.26
(2)	SBP	0.72	0.17	0.75	0.14	0.35	0.25
	DBP	0.77	0.16	0.81	0.11	0.40	0.29
(3)	SBP	0.77	0.15	0.81	0.11	0.38	0.29
	DBP	0.72	0.17	0.75	0.14	0.33	0.25
(4)	SBP	0.77	0.16	0.81	0.11	0.41	0.29
	DBP	0.72	0.17	0.75	0.14	0.37	0.26
(5)	SBP	0.82	0.16	0.85	0.11	0.49	0.26
	DBP	0.75	0.17	0.78	0.14	0.46	0.26
(6)	SBP	0.82	0.13	0.85	0.08	0.72	0.20
	DBP	0.78	0.14	0.80	0.12	0.70	0.19
(7)	SBP	0.82	0.13	0.85	0.08	0.71	0.21
	DBP	0.78	0.14	0.80	0.12	0.69	0.20

The use of $\mathbf{PTT_{onset}}$ leads to higher $\overline{R^2}$ and lower SD in every model tested, therefore it was deemed the best distal reference point from PPG cycle for the purpose of estimating SBP and DBP, and it will be used to compute the all the results in the following sections of this work.

To evaluate the influence of the device in the BP estimation, the calibration phase is performed using both devices (A and B) for each subject. The calibration results, using $\mathbf{PTT_{onset}}$, for devices A (previously presented in Table 3.4) and B can be observed in Table 3.5 and Figure 3.9.

The ANOVA test was used to test the null hypotheses ($H_0 : \mu_{(1)} = \mu_{(2)} = ... = \mu_{(7)}$), in contrast with the alternative hypothesis H_1 where at least one mean is statistically different from the remaining. Since $F = 2.144 < F_{crit} = 2.167$ ($p - value = 0.052 > 0.050$), for SBP, and $F = 0.733 < F_{crit} = 2.167$ ($p - value = 0.624 > 0.050$), for DBP, the null hypothesis can not be rejected at the level of significance $\alpha = 0.05$. There was not enough evidence to conclude that the coefficient of determination mean between models

Table 3.5: Coefficient of determination mean ($\overline{R^2}$) and SD correspondent to devices A and B calibration for all subjects

Device	Model	SBP		DBP	
		$\overline{R^2}$	SD	$\overline{R^2}$	SD
A	(1)	0.81	0.11	0.75	0.14
	(2)	0.75	0.14	0.81	0.11
	(3)	0.81	0.11	0.75	0.14
	(4)	0.81	0.11	0.75	0.14
	(5)	0.85	0.11	0.78	0.14
	(6)	0.85	0.08	0.80	0.12
	(7)	0.85	0.08	0.80	0.12
B	(1)	0.52	0.29	0.46	0.26
	(2)	0.46	0.25	0.52	0.28
	(3)	0.53	0.28	0.47	0.25
	(4)	0.51	0.29	0.46	0.26
	(5)	0.61	0.27	0.56	0.20
	(6)	0.64	0.24	0.65	0.21
	(7)	0.65	0.24	0.65	0.20

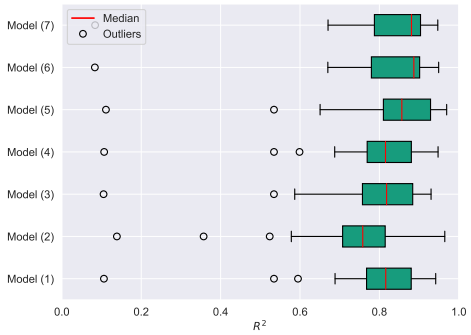

(a) SBP (Device A)

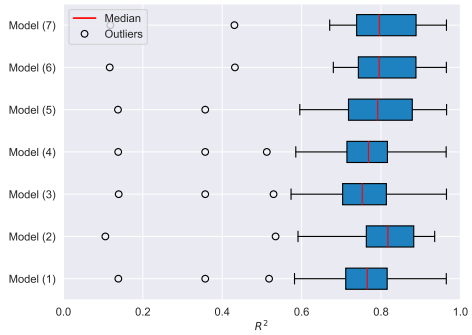

(b) DBP (Device A)

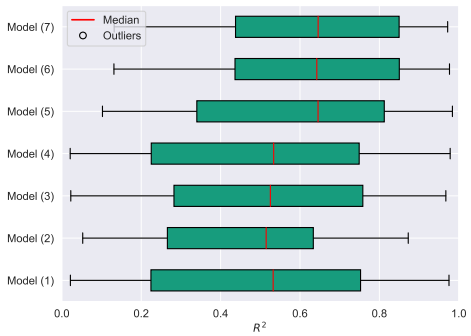

(c) SBP (Device B)

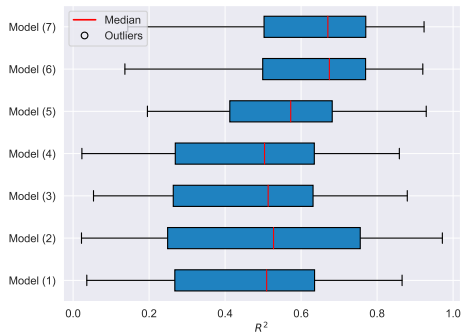

(d) DBP (Device B)

Figure 3.9: Boxplot of the coefficient of determination obtained for calibration of SBP and DBP in all subjects

differ for both SBP and DBP. The model (7) presented the highest average coefficient of determination for both SBP and DBP and devices A and B thus, only the results for this model will be presented in the following sub-sections.

3.3.2 Static and Dynamic Tests

Table 3.6: Results obtained from data collected in Static and Dynamic tests

Device	Model	(ME ± SD) (mmHg)	(MAE ± SD) (mmHg)	RMSE (mmHg)	R [a]
A	SBP	0.1 ± 4.1	2.9 ± 2.9	4.1	0.95
	DBP	-1.2 ± 3.8	3.1 ± 2.4	4.0	0.91
B	SBP	-1.4 ± 5.9	4.3 ± 4.3	6.0	0.90
	DBP	-2.0 ± 4.3	3.7 ± 3.0	4.7	0.89

[a] Coefficient of correlation between measured and estimated BP values

Table 3.7: Results obtained from data collected in Static and Dynamic tests (presented separately for device A)

Test	Model	(MAE ± SD) (mmHg)	RMSE (mmHg)
Static	SBP	2.5 ± 3.0	3.9
	DBP	2.7 ± 2.0	3.4
Dynamic	SBP	3.3 ± 2.9	4.4
	DBP	3.5 ± 2.7	4.4

The results obtained from the overall data are presented in Table 3.6, the results are presented separately for static and dynamic test in table 3.7 and Figure 3.10 where different colors and markers are used to represent different users and test type (static and dynamic).

From this results, it is possible to understand that the device A led to better results in both SBP and DBP. This may have been caused by the type of PPG sensor used in the device B. The wavelength used in this sensor can only evaluate the volume changes in the most superficial vessels; in cases where the room temperature is slightly lower, the signal to noise ratio dramatically reduces due to vasoconstriction. This can cause misidentification of the important points in PPG signal. This factor may explain the differences between both devices. On the table 3.7 where the results are presented separately for static and dynamic tests, the estimation of the BP in the dynamic test was worse when compared to the static test, leading to higher MAE and RMSE. This can be caused by the higher number of BP points referent to static position when compared to the dynamic position in the calibration process, since the isometric exercise is only performed until fatigue.

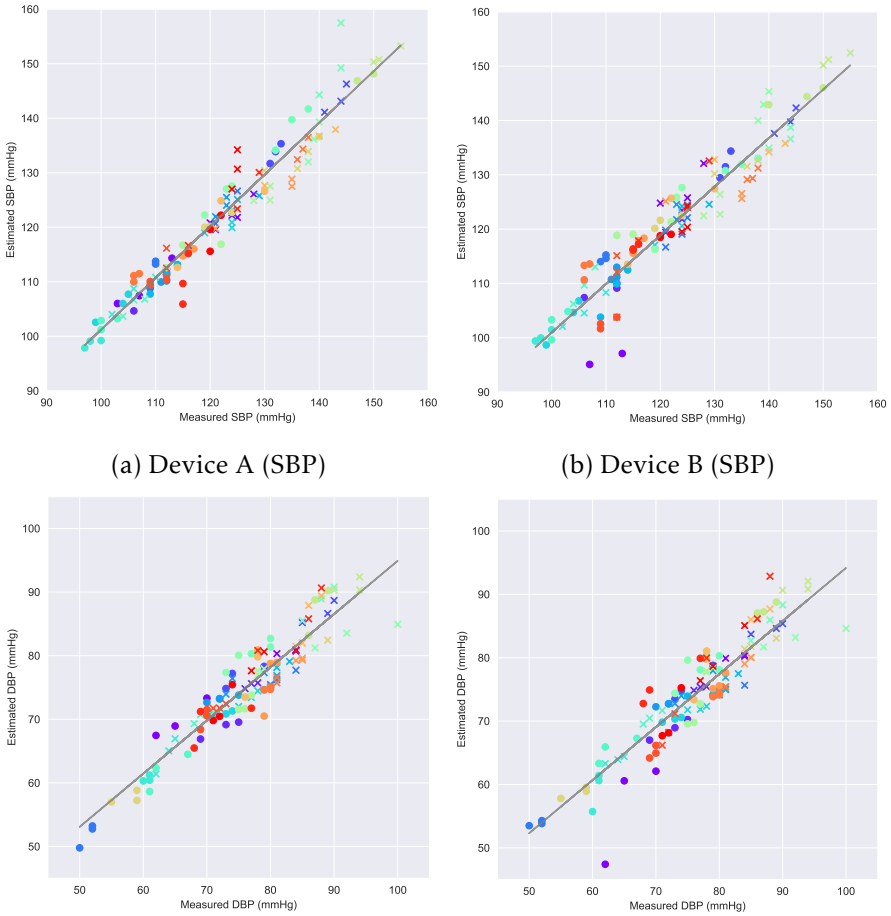

(a) Device A (SBP)

(b) Device B (SBP)

(c) Device A (DBP)

(d) Device B (DBP)

Figure 3.10: Results after calibration. Each color represents different subjects. Bullet points represent data from static test and crosses represent data from dynamic test

3.3.3 Follow-up Test

The calibration was re-tested in a follow-up test, with dataset acquired after a period of time between one and two weeks from the first acquisition. The main objective of this follow-up test was to infer how well the calibration can hold its capability of estimation the BP. The results of this test can be found in Figure 3.11 and Table 3.8.

These results indicate that the calibration for each subject loose quality over time, and, due to this factor, an eventual re-calibration is necessary if the objective is to perform long term BP estimations.

Table 3.8: Follow-up Test results obtained from data collected in Static and Dynamic tests

Device	Model	ME ± SD (mmHg)	MAE ± SD (mmHg)	RMSE (mmHg)	R [a]
A	SBP	1.8 ± 6.7	4.3 ± 4.5	6.0	0.90
	DBP	-2.4 ± 5.9	5.2 ± 3.7	9.2	0.76
B	SBP	-1.3 ± 9.2	7.8 ± 5.0	9.3	0.81
	DBP	-3.5 ± 6.7	6.1 ± 4.4	7.5	0.69

[a] Coefficient of correlation between measured and estimated BP values

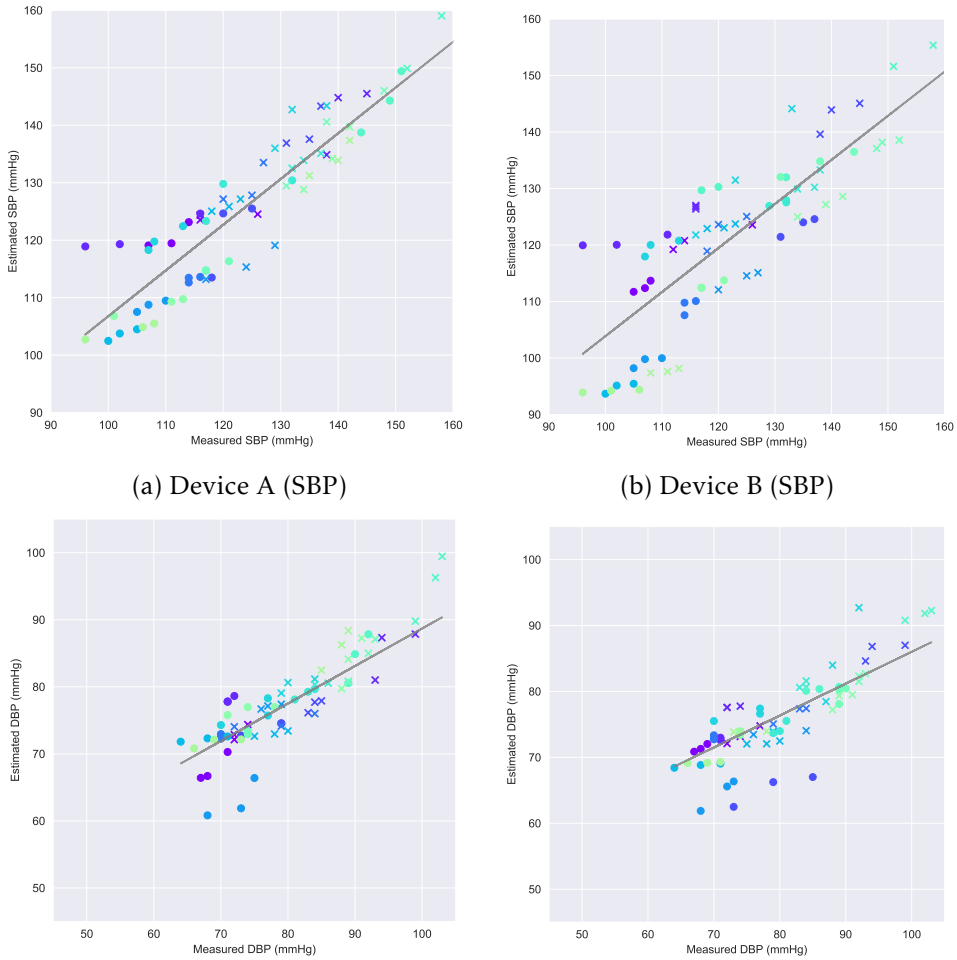

(a) Device A (SBP)

(b) Device B (SBP)

(c) Device A (DBP)

(d) Device B (DBP)

Figure 3.11: Follow-up Test results. Each color represents different subjects. Bullet points represent data from static test. Crosses represent data from dynamic test

3.4 Discussion

The direct comparison between different scientific works is not always possible, since different authors evaluate their systems based in different metrics and test protocols. In this work the results were evaluated following as much as possible the Standard IEEE 1708-2014, this standard was created in order to standardize the evaluation of these devices.

Table 3.9: Machine learning comparison (SBP)

Studies	**MAE ± SD** (mmHg)	**RMSE** (mmHg)
This Work	2.9 ± 2.9	4.1
Chen *et al.* [47]	-	-
Ding *et al.* [7]	4.09 ± -	-
Carek *et al.* [68]	-	2.9

Table 3.10: Machine learning comparison (DBP)

Studies	**MAE ± SD** (mmHg)	**RMSE** (mmHg)
This Work	3.1 ± 2.4	4.0
Chen *et al.* [47]	1.4 ± -	7.5
Ding *et al.* [7]	3.18 ± -	-
Carek *et al.* [68]	-	4.8

In the implemented method used to estimate the BP using biophysical models, the calibration was performed with an automatic oscillometric device instead of using an invasive method, like in the approach tested by Chen *et al.*, or manual measurements using a conventional mercury sphygmomanometer. This enabled the scalability of the system for final users and can be adapted for ambulatory scenarios. Another difference is the exercise performed in the calibration procedure (isometric leg exercise). In most studies, the BP was varied by medication or via cardiovascular based exercises, that implies a large amount of subject motion, leading to low quality signals and impossibility to be performed in subjects that suffer from motor difficulties. The system was evaluated following as much as possible with the criteria presented in IEEE Standard for Wearable Cuffless Blood Pressure Measuring Devices [72]. As previously mentioned, since the ground truth for BP in the studies presented in tables 3.9 and 3.10 are not homogeneous, a direct performance comparison between the method tested in this work and the methods in bibliography is limited. However, it is possible to conclude that the developed work had a similar performance when compared to other studies [7, 47, 68].

Table 3.11: ANSI/AAMI SP10 and Standard 1708-2014 evaluation criteria [72, 73]

MAE (mmHg)	**ANSI/AAMI SP10**	**Recommended grade**
≤ 5	pass	A
5 - 6	pass or fail	B
6 - 7	mostly fail, less pass	C
≥ 7	fail	D

Using all data as indicated in the standard (static test, test with BP change from the calibration point, and test after a certain period of time from calibration), both devices (A and B) were classified with recommended grade A if used right after calibration.

Chapter 4

Blood Pressure Estimation Using Machine Learning

To overcome some of the BP estimation disadvantages using the method presented in chapter 3, like the need of calibration and re-calibration, a different approach, using machine learning methods, is presented and explained in this chapter. This part of the work was developed as a proof of concept using a public dataset.

4.1 State of the Art

Several studies have been published recently reporting the use machine learning methods to estimate BP.

In 2013, Kurylyak *et al.* [74] used an Artificial NN and a set of 21 features, including HR, the times of systolic and diastolic parts of the PPG cycle, as well as different widths at different heights, extracted from subjects present in medical information mart for intensive care (MIMIC) database. In total, 15000 PPG cycles with the corresponding BP values were used, although there are no information about how many subjects were used. The training and test sets were randomly selected based on instances (70% for training, 15% for validation and 15% for testing). This approach had a MAE of 3.80 ± 3.46 mmHg for SBP and 2.21 ± 2.09 mmHg for DBP.

In 2017, Kachuee *et al.* [75] proposed a framework to estimate the BP through two types of features from the ECG and PPG signals, physiological parameters, like PAT based features, HR and inflection point area ratio, and whole-based features, that are features that result from parsing a window containing various cardiac cycles. A total of 10 features from roughly 1000 unique subjects from MIMIC II database were used to train/test five different learners (linear regression, decision tree, support vector machine, AdaBoost and RF). This framework had a MAE ± SD of 11.17 ± 10.09 mmHg and 5.35 ± 6.14 mmHg for

SBP using RF (best performance learner in the study). An additional step of calibration was added to the calibration-free method, which improved the results to 8.21 ± 5.45 mmHg and 4.31 ± 3.52 mmHg MAE ± SD, respectively. No considerations were made about PPG/ECG desynchronization.

In 2018, Wang *et al.* [76] proposed a method based only in PPG extracted features. The features were extracted using the multitaper method, and the BP estimation was performed using an NN. A total number of 72 subjects from MIMIC database were used in this approach, the PPG signals of each subject were divided by cycle, and a total of 22 features were calculated for each cycle, two morphological features (systolic upstroke time and diastolic time) and twenty spectral features (extracted using multitaper method). The data was randomly split in 70% of the instances for training, 15% for validation and 15% for testing. The proposed method results in mean differences between the estimated and measured BP, of -0.0217 ± 4.8950 mmHg for SBP and 0.0975 ± 2.9160 for DBP, and MAE of 4.02 ± 2.79 mmHg and 2.27 ± 1.82 mmHg for both SBP and DBP respectively.

In the same year, Radha *et al.* [77] tested a method to estimate SBP based in long- and short term memory networks (LSTM), dense networks, RF and linear regression models. Features based on heart rate variability and pulse morphology were extracted from the PPG signal, and used to train the models. The models were trained and tested using a custom dataset acquired at Philips Research laboratory. A total of 110 healthy volunteers aged between 18 and 65 years, were asked to wear a wrist band containing a green PPG sensor and a triaxial accelerometer, as well as a clinically validated ambulatory BP monitor. A total of 226 days of PPG data, and 6629 valid reference BP measurements were acquired. The results demonstrated that the RF with 32 trees outperformed the other tested models with a RMSE of 7.86 ± 1.57 mmHg for SBP, in DBP the dense network with 8 perceptrons had slightly better results, with RMSE of 6.49 ± 1.59 mmHg. Contrary to what was done in the other presented studies, the split between the training/test sets was performed by subject.

4.2 Materials and Methods

The process of estimating the BP using machine learning is similar to the process that uses biophysical models. Some core differences should be noted, first, since the process of data acquisition cannot be controlled, the acquired signals can be affected by intense noise, motion artifacts and portions of the data where one or more signals are not available, a pre-processing phase was implemented with the aim of overcoming these problems. Other core difference is the data used to train the machine learning models, in the approach using biophysical models the BP is measured using a common oscillometric device that results in low frequency measurements, in contrast to the intra-arterial BP data used in the approach presented in this chapter that can be used to identify the BP in each heart cycle.

4.2.1 MIMIC III Database

The MIMIC III is a freely available database that contains data from 53 423 distinct hospital admissions for adult patients (+16 years old) who stayed in critical care units of the Beth Israel Deaconess Medical Center in Boston, Massachusetts, between 2001 and 2012 [78, 79].

The database contains a variety of information, like hourly measurements of vital signs, lab test results, medical procedures, medications, mortality information, and other types of information. A subset of patients also contains several physiological signals (MIMIC-III Waveform Database), in some cases during hours, such as ECG, PPG, intra arterial BP, among others. These signals were acquired from bedside monitors, and not all signals are available for all of the subjects in this subset. A full description of the collection procedure and the hardware used is not available, but since all data were collected in medical environment, it is expected that they have been collected using standard medical protocols and hardware, this way, it is expected that the PPG signal was acquired in the finger and the intra arterial BP with a transducer inside the radial artery. It is also important to note that only a small portion of the MIMIC-III Waveform Database are linked to the MIMIC III, because of that, most of the data does not have information about subject's age and gender. In addition, due to privacy concerns subjects with more than 89 years of age were shifted to hide their true age and comply with HIPAA regulations [78]. It is neither possible to ensure an alignment inter-signals. The waveform data contains unknown filtering delays and/or unknown inter-channel delays, which may not be constant at a given record and between different subjects. This limitation makes it impossible to use inter-signals features.

In this work, due to hardware limitations, mostly memory size constrains, a random subset of 1156 patients, containing ECG, PPG and BP signals, was selected from MIMIC-III Waveform Database.

The SBP and DBP histograms from the selected subset of data can be found in the Figure 4.1.

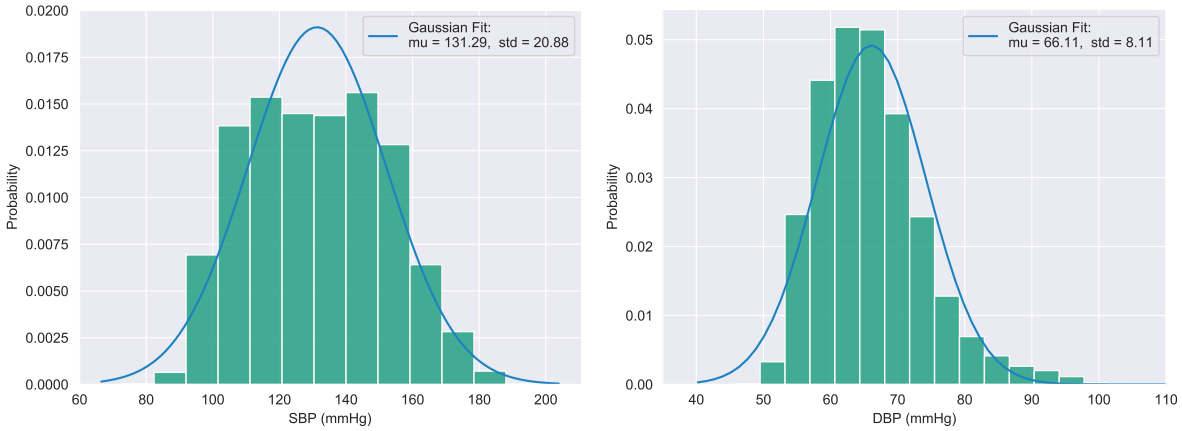

(a) SBP histogram

(b) DBP histogram

Figure 4.1: Histogram of the BP data for the 1156 patients randomly selected from MIMIC III database

4.2.2 Pre-processing

First the PPG and ECG signals are filtered using the same procedure described in chapter 3, to remove high frequency noise. The BP signal is kept unfiltered since this process influence the amplitude values of the signal.

4.2.2.1 BP Signal Cleaning

The BP signal is divided in windows of 5 seconds, and the maximum (that corresponds to the maximum SBP) and the minimum (that corresponds to the minimum DBP) of each window is calculated. The windows where the parameters do not meet the physiological limit values are removed, this allows the removal of portions of the signal where the pressure suddenly rises due to subject movement. Those parameters were defined as [80]:

- 60 mmHg < Maximum SBP < 220 mmHg;
- 30 mmHg < Maximum DBP < 150 mmHg;
- SBP - DBP > 20 mmHg.

4.2.2.2 PPG and ECG hard Noise Cleaning

The process of cleaning both PPG and ECG signals is based on the periodicity of these signals in time, and the procedure is the same for both signals.

The portion of the signal inside a 5 second sliding window is used to calculate the autocorrelation signal. Two output examples are represented in figures 4.2 and 4.3.

It is possible to observe that, since the ECG and PPG signals are relatively periodic, the autocorrelation signal does not have a significant decrease for lower values of lag. Conversely, in signals affected by severe noise, small values of lag lead to higher decrease in the autocorrelation signal.

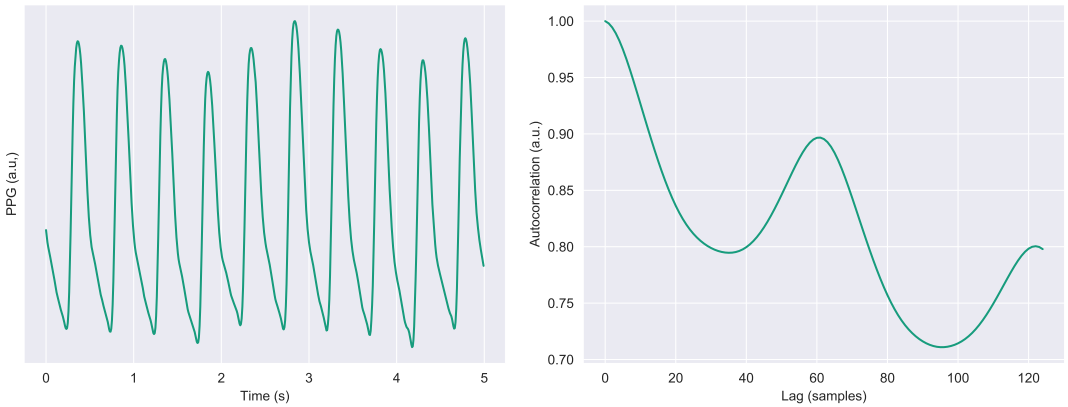

(a) PPG signal (b) Autocorrelation signal

Figure 4.2: Good quality PPG Signal and respective autocorrelation signal

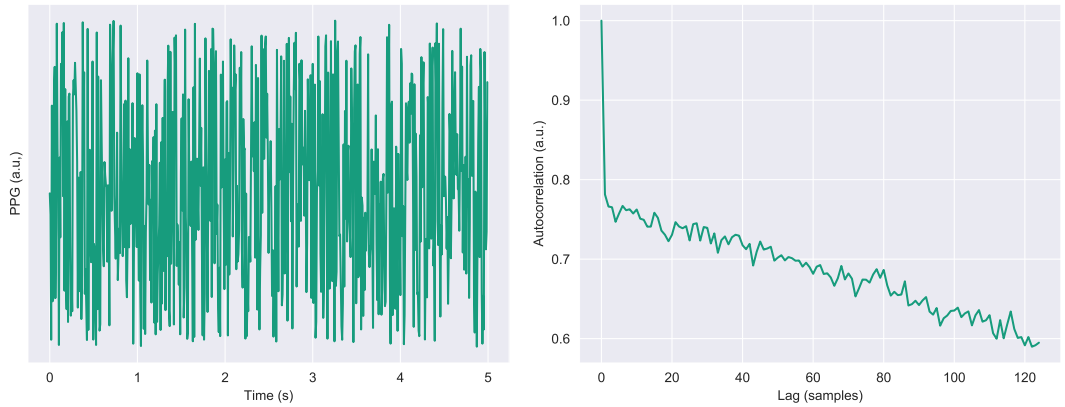

(a) PPG signal (b) Autocorrelation signal

Figure 4.3: Noisy PPG Signal and respective autocorrelation signal

The signal is removed if the autocorrelation coefficient with a lag of 8 samples is lower than 0.85. This values were used based on empirical observations.

4.2.2.3 Template Cleaning

Although the signals are relatively free of high frequency intense noise at this stage, some zones of the signal can have low quality segments due to factors like motion artifacts and momentary poor conductivity between the surface of the body and the sensor. This way, a robust method to detect and remove the zones with lower quality signal is necessary.

It was achieved based on a template creation and comparison technique, in this section it is described with the PPG signal, but is equally used with the ECG. The process can be described as:

1. **Fiducial Point Detection:** The first part of the process is to identify the points that mark the beginning of the PPG cycle (a complete description can be found in chapter 3).

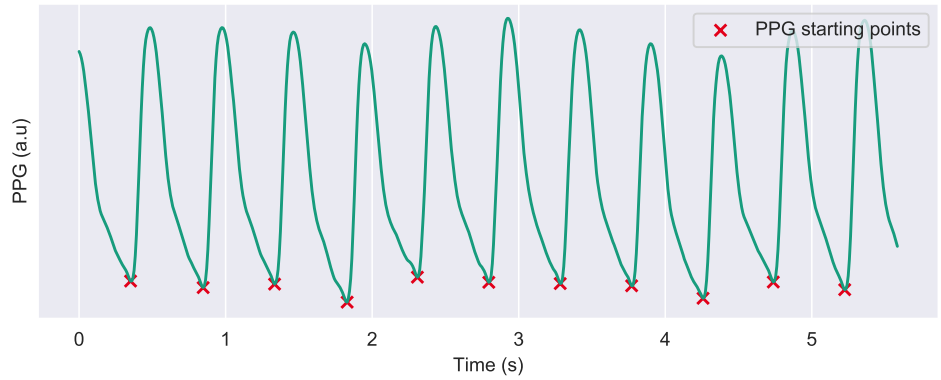

Figure 4.4: PPG signal and detected starting points of each cycle

2. **Template Creation:** A 30 seconds sliding windows with an overlap of 1 second is then used to calculate the PPG template. It is calculated as the mean of all cycles detected in that windows (one for each beginning point detected in the fidutial point detection phase). For simplification all cycles are considered to have the same length on that window, equal to the lag associated with the first maximum of the autocorrelation signal.

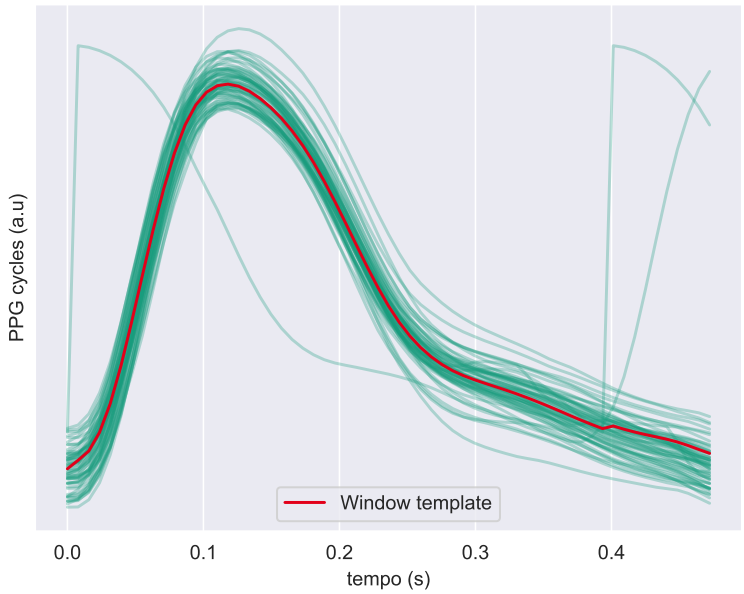

Figure 4.5: 30 seconds window PPG cycles and generated template

3. **Cycle/Template Comparison:** Each cycle on the windows is compared with the window template using the Pearson correlation coefficient to measure the similarity between cycles, and using the correlation between time-warped cycles (that result from DTW) and the template. A threshold of 0.9, defined empirically, is used to determine if the PPG cycles have good quality, the cycles with coefficients lower

than 0.9 are discarded. If more than 50% of the cycles are considered bad quality cycles, the entire window is removed.

This approach results in a trade off between signal quality fed into the regression model and the frequency of new BP estimations. The 30 seconds window was empirically chosen so that the portion of the 30 seconds window contains enough cardiac cycles to create the template, maintaining, however, a relatively high measurement frequency when compared with the current methods. An example of this pre-processing phase can be seen in image 4.6.

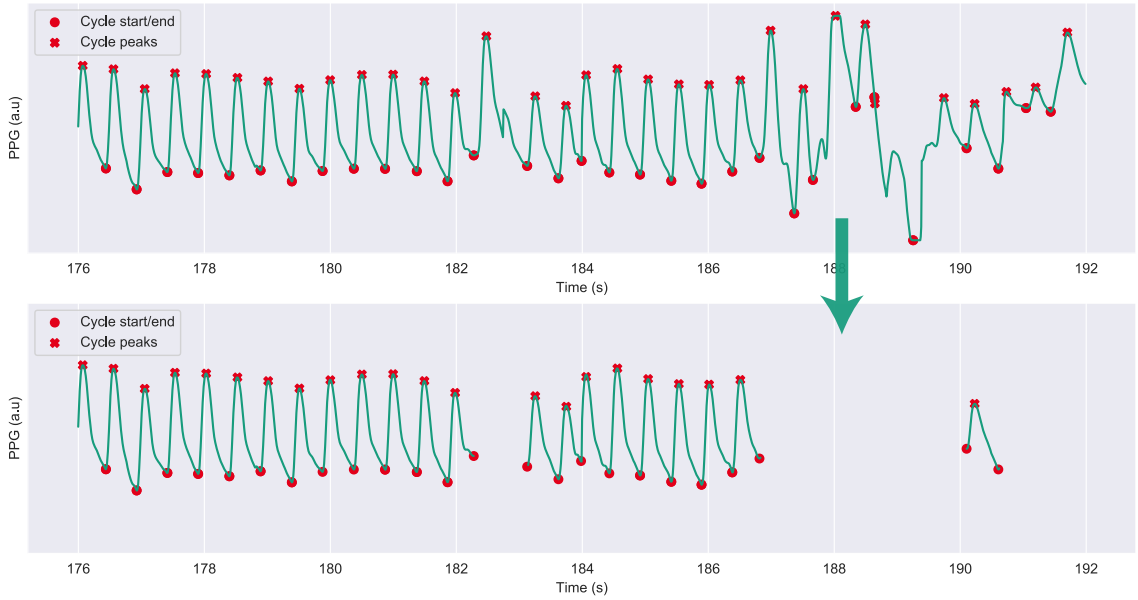

Figure 4.6: Pre-processing phase example

4.2.3 Features Extraction

Several features are selected from ECG and PPG signals, a brief explanation of each feature can be seen in table 4.1. The presented features are calculated for each PPG cycle, associated with the respective SBP and DBP and vertically scaled between 0 and 1.

The time series feature extraction library (TSFEL) is a feature extraction library developed by Fraunhofer AICOS with the objective of assist researchers on exploratory feature extraction tasks on time series [1]. It is used in this work to automatically extracts more than 50 different features on the statistical, temporal and spectral domains (Table 4.2).

[1] Avalible in `github.com/fraunhoferportugal/tsfel`

[2] $f(t) = a_1 e^{-(\frac{t-a_2}{a_3})^2} + b_1 e^{-(\frac{t-b_2}{b_3})^2}$

Table 4.1: Used Features

Signal	Feature	Description
ECG	RR	time between R peaks of the present cycle and the previous cycle
PPG	t_1	time between the start and the onset points of the cycle
PPG	t_2	time between the start and the maximum points of the cycle
PPG	t_3	time between the start and the final points of the cycle
PPG	t_4	time between the maximum of the cycle and the minimum gradient between the maximum and the end of the cycle
PPG	t_5	time between the maximum of the cycle and the minimum gradient between the maximum and the end of the cycle
PPG	t_6	time between the maximum of the cycle and the maximum of the second order gradient between the maximum and the end of the cycle
PPG	A_{total}	total area under the cycle curve
PPG	A_1	ratio between the area under the curve between the starting point and the onset point, and the total area
PPG	A_2	ratio between the area under the curve between the starting point and the maximum point, and the total area
PPG	A_3	ratio between the area under the curve between the maximum point and the end point, and the total area
PPG	a_1, a_2, a_3 b_1, b_2, b_3	constants of the function $f(t)$ [2] fitted to the cycle
PPG	W_{25}	width 25% hight
PPG	W_{50}	width 50% hight
PPG	W_{75}	width 75% hight
PPG		+ Features from TSFEL

Table 4.2: TSFEL features examples

Domain	Feature	Description
Statistical	Skewness	measures the asymmetry of the signal distribution
	Kurtosis	measures the distribution shape around a normal distribution
	Histogram	plots the number of members for each bin against a total given number of bins
	Mean	measures the signal arithmetic mean
	Variance	measures the dispersion of the signal value
	Standard Deviation	measures the dispersion of the signal values
	Interquartile Range	computes the difference between the upper and lower quartile
Temporal	Max	computes the signal maximum value
	Min	computes the signal minimum value
	Centroid	computes the arithmetic mean position of all the signal points
	Root Mean Square	computes the square root of the arithmetic mean of the square of the signal values
	Median Absolute Deviation	computes the median distance between each data value and the signal median value
	Zero Crossing Rate	computes the rate at which the signal sign changes
	Autocorrelation	computes the correlation of a signal with a lagged version of itself
	Linear Regression	computes the linear regression of the signal
Spectral	Max Frequency	computes where the FFT reaches its 95% of distribution
	Median Frequency	computes where the FFT reaches its 50% of distribution
	Fundamental Frequency	computes the frequency corresponding to the greatest common divisor of all the frequency components in the signal

Max Power Spectrum	computes the maximum value of the power spectrum density along a given axis
Total Energy	computes the total energy of the signal given by the squared sum of the spectral coefficients normalised by the length of the sample windows
Spectral Centroid	computes the weighted mean position of the signal frequencies distribution and their probability
Spectral Spread	measures the variance of the signal frequencies asymmetry distribution
Spectral Skewness	measures the asymmetry of the signal frequencies distribution
Spectral Kurtosis	measures the signal frequencies distribution shape around a normal distribution
Spectral Slope	measures how quickly the spectrum decreases towards the high frequencies
Spectral Decrease	measures the decrease on the spectral amplitude though its linear regression computation
Spectral Roll On	computes the frequency so that 5% of the signal energy is contained below of this value
Spectral Roll Off	computes the frequency so that 95% of the signal energy is contained below of this value
Curve Distance	computes the euclidean distance of the signal's cumulative sum of the FFT elements to the linear regression
Spectral Variation	computes the spectral variance from the cross-correlation of two consecutive amplitude spectra

Some feature from TSFEL have no relevance in the context of this work, one example is the maximum of the cycle. Since the cycle is always scaled between 0 and 1, and the amplitude of the PPG can vary depending on hardware factors, this feature does not add any information. This way the features with zero variance are removed.

4.2.4 Machine Learning

The calculated features are used to train three machine learning models implemented in Scikit-learn [58], a NN, a AdaBoost, and a RF.

Since the objective is to predict the BP in new users without a calibration phase, the dataset is split based on users, instead of instances. Following this premise the dataset is divided in 7 groups of 152 subjects (for 7-fold cross-validation) with a total of 1064 subjects, this represents that nearly 14% of the data is used as testing set. This is in line with the recommended values by the literature [81] of between 10% and 20%. The training is performed with 6 groups and the remaining group is reserved for testing, the procedure is repeated until every group is used as testing set, the output result is the mean of all iterations.

An intermediate phase of feature scaling (to mean zero and unit variance) is also performed, because methods like NN are sensitive to the input data magnitude. This phase should be executed separately in the test and training group, so there is no leak of information (mean and standard deviation) between the sets.

The last step before training the models is dimensionality reduction using PCA algorithm. The objective is to understand whether the PCA use leads to an indirect improvement, due to faster convergence to the solution, caused by the reduction on the number of features. The number of principal components is selected based on the desired cumulative explained variance (95% in this work).

4.3 Results

The use of PCA algorithm led to a 3.6 times faster training phase, but it did not contribute to the accuracy improvement, which is considered the main objective. In both tests, before and after PCA, the NN performed better in estimating SBP and DBP (Table 4.3 and 4.4) with a MAE of 3.59 ± 4.29 mmHg and 2.02 ± 2.50 mmHg, respectively. It is also possible to observe that, in contrast with the BP estimation using biophysical models, the system performed better at estimating DBP rather then SBP.

Table 4.3: Results before PCA

Model	**SBP**		**DBP**	
	MAE ± SD (mmHg)	RMSE (mmHg)	MAE ± SD (mmHg)	RMSE (mmHg)
NN	3.6 ± 4.3	5.6	2.0 ± 2.5	3.2
RF	4.3 ± 4.6	6.3	2.3 ± 2.6	3.4
AdaBoost	12.2 ± 8.2	14.8	8.8 ± 5.4	10.4

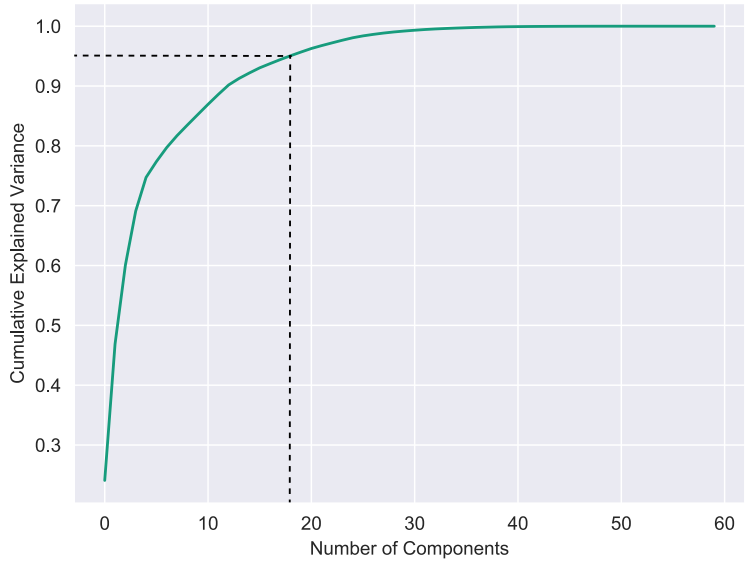

Figure 4.7: Cumulative explained variance as a function of number of components, the number of principal components (18) is selected based on the desired cumulative explained variance (95%)

Table 4.4: Results after PCA

Model	**SBP**		**DBP**	
	MAE ± SD (mmHg)	RMSE (mmHg)	MAE ± SD (mmHg)	RMSE (mmHg)
NN	5.1 ± 5.1	7.2	2.7 ± 2.9	4.0
RF	5.1 ± 5.4	7.4	2.7 ± 3.0	4.1
AdaBoost	13.5 ± 9.1	16.3	7.7 ± 4.9	9.2

The results indicate that the method presented in this chapter is capable of estimate BP without the requirements associated with the use of biophysical models to estimate BP, like the need of a calibration process to each user

4.4 Discussion

The approach presented in this chapter cannot be evaluated using the same grading system, since the data used cannot be controlled in terms of BP variations. Although, several studies have used the same database or previous versions, facilitating the process of comparison between them. The proposed method had lower mean absolute error for both SBP and DBP, when compared with other works (Table 4.5 and 4.6).

It is important to note that only in the studies performed by Radha *et al.*, Kachuee *et al.*, and in this work, the splitting between training and test sets was made based on subjects, instead of instances. The splitting based on instances lead to better results, but it is a weaker evaluator, because instances from the same subject can be used both for

training and testing.

Table 4.5: Machine learning comparison (SBP)

Studies	**MAE ± SD** (mmHg)	**RMSE** (mmHg)
This Work	3.6± 4.3	5.6
Kurylyak *et al.* [74]	3.80 ± 3.46	-
Kachuee *et al.* [75]	11.17 ± 10.09	-
Wang *et al.* [76]	4.02 ± 2.79	-
Radha *et al.* [77]	-	7.86

Table 4.6: Machine learning comparison (DBP)

Studies	**MAE ± SD** (mmHg)	**RMSE** (mmHg)
This Work	2.0 ± 2.5	3.2
Kurylyak *et al.* [74]	2.21 ± 2.09	-
Kachuee *et al.* [75]	5.35 ± 6.14	-
Wang *et al.* [76]	2.27 ± 1.82	-
Radha *et al.* [77]	-	6.49

Chapter 5

Conclusion

In order to optimize the cuffless BP measurements in the future, and understand the advantages and disadvantages of the methods developed in this work, it is important to compare them with previous works in the field, as well as proposed future changes than can lead to better results or a better system.

5.1 Overall discussion and Conclusions

Hypertension is a significant risk factor in several cardiovascular diseases, it is estimated that 13% of the world's deaths are directly or indirectly linked to this condition. The current methods to measure BP, such as oscillometric devices, have some disadvantages, that hinder the correct BP measurement in ambulatory conditions, during sleep, exercise, or when continuous values are needed.

This work was developed with the main objective of developing a method that could be used to measure BP without the usual cuff used in the current standard devices.

Two different solutions were proposed for estimating BP from ECG and PPG signals, one based in biophysical models and the other using machine learning methods.

The first approach uses biophysical modelling of the arterial blood flow to estimate BP. The developed system can be described in four stages, first the physiological signals are pre-processed, with the objective of removing high frequency noise and correct zones of the PPG signal where the sensor saturate. Then the PTT is calculated using as time reference the R peaks from ECG (proximal reference), and different points from PPG (distal references). The use of the pair (PPG, ECG) to calculate PTT makes the process more robust, when compared with (PPG,PPG) configuration or equivalent, because PPG signal can be hard to acquire in some locations, like in extremely warm or cold environments, and it is greatly affected by motion artifacts. The third phase is the calibration of

the system using the pairs (PTT, BP), the calibration is performed individually for each subject, and then the BP can be estimated using the new PTT values and the calibrated model.

This process was performed in parallel with two different devices, and for seven different models previously proposed in the literature [49–56], in a total of 20 subjects in laboratory conditions. To evaluate the proposed method a test dataset was acquired for each subject, this dataset includes three measurements in seated static position, three measurements performing an isometric exercise to vary the BP, and a repetition of both two weeks later, resulting in a total of 12 test points for subject. This was made based in the indications present in the IEEE Standard for Wearable Cuffless Blood Pressure Measuring Devices.

It was possible to take some valuable conclusions from this approach, first the results indicate that it is possible to successfully estimate BP using just PTT following a calibration procedure. I was also observed that the calibration looses quality over time, due to variations in physiological constants, like arteries Young's modulus, precluding the application of this approach for long periods of time without performing regular re-calibrations. The comparison of the results between the two tested devices indicates that the used hardware plays an important role in the system accuracy, an example is the type of PPG sensor (transmittance *versus* reflectance). Although the reflectance version of the sensor is more versatile because it can be used in location like the wrist, the resultant signal is heavily affected by superficial arteries vasoconstriction in lower ambient temperatures, leading to worse results.

The second approach is based on application of machine learning techniques to a large publicly available database of physiological signals from ICU patients, with the objective of overcoming some of the limitations inherent to the previous method, such as the necessity of calibration and re-calibrations.

In contrast to the first approach, where was possible to acquire the needed data, the use of a clinical database implies some added difficulties, such as, the higher presence of noise and motion artifacts, and the possibility that not all of the signals are available for all patients and the whole duration of the record. This creates the need for additional data pre-processing steps, namely three different pre-processment stages were applied, first the portion of data where the BP signal had impossible physiological values due to subject motion while acquiring the intra arterial BP (e.g SBP $>$ 220 mmHg) was removed, then the portions with high noise were identified and removed using the autocorrelation signal. The final step was to select only the high quality cycles from ECG and PPG, *i.e* the cycles that are not influenced by motion artifacts, and other conditions that change the general shape of the cycles. This is achieved by comparing each cycle with a template calculated using all cycles in a windows of time. The resultant signals were then used to calculate the a total of 58 features, and used to train three different machine learning methods.

The results indicate that the proposed method can be successfully used to estimate

BP, outperforming the similar studies, this shows the potential of this technology in the current field.

It is possible to conclude that both approaches have the potential to be used to solve the proposed problem of measuring the BP without the cuff need. However, there is a fundamental difference between them that should be noted and can influence the fields of application of the presented solutions. While the approach using biophysical models requires an initial process of calibration and future re-calibrations to maintain the accuracy over time, the solution using machine learning methods does not use any calibration phase, it makes the system more ready to use, with the potential to be used in passive health monitoring systems, like smartwatches. While the first solution can be used during hospitalization to estimate the BP between the already performed periodic traditional measurements of BP.

It is also important to mention that there are some limitations that may have influenced the results, the accuracy of the first approach are highly influenced by the accuracy of the traditional device to measure the BP, and by the perfect synchronisation between the acquired signals (ECG and PPG) and the BP values. Due to this factor it is crucial to ensure the quality of the used material and the synchronization between data, so that the results are consistent. In the second study it is important to identify the lack of information about the sensors used to acquire the signals, and the impossibility of ensure intra-subject variability of BP for a more robust training phase.

5.2 Future Work

Although the developed work shows promising results, some additional investigation and changes are foreseen to improve it.

In the first approach the system can be simplified in a more compact and ready to use system, this would allow a more comfortable and fast process of data acquisition in environments outside the lab, contributing to a higher variety in the acquired data. Changes can also be performed in the signal pre-processment stage, similar to the equivalent stage in the second approach using machine learning, this will make the overall system more robust, and better adapted for real world scenarios.

The second approach has more room for future improvements, since it is a recent method in bibliography, and was developed mainly as a proof of concept in this work. First, and to complement the work performed, a validation step should be performed, to fine tune the hyperparameters of the different machine learning models. The proposed method can also be adapted to work with the type of data acquired in the first approach using, for example, transfer learning. It would be interesting to test if similar results can be obtained using non-invasive and low frequency BP measurements, which could make the process of custom made database acquisition easier. The method can also be easily adapted to work only with the PPG signal, since the ECG signal is only used in this work to correct PPG fiducial points, and to calculate only one feature. With this small

change, a future final device can be more user-friendly and be adapted as a watch type device. Future works can also explore the developments in the deep learning field, and apply it to test approaches that use deep learning to select the portions of the signals with enough quality to be used to estimate the BP, or/and use it to remove the feature extraction phase.

Bibliography

[1] WHO Regional Office for Europe. "High blood pressure -Country experiences and effective interventions utilized across the European Region." In: *Who* (2013), pp. 1–30.

[2] G. Stevens, M. Mascarenhas, and C. Mathers. "Global health risks: progress and challenges." In: *Bulletin of the World Health Organization* 87.9 (2009), pp. 646–646. ISSN: 00429686. DOI: 10.2471/BLT.09.070565. arXiv: 9789241563871.

[3] A. P. Rodrigues et al. "Prevalência de hipertensão arterial em Portugal : resultados do Primeiro Inquérito Nacional com Exame Físico (INSEF 2015)." In: *Boletim Epidemiológico Observações* 6.9 (2017), pp. 11–14. ISSN: 0160-7715 (Print). DOI: 10.1107/S0907444905036759.

[4] E. Wilkins et al. "European Cardiovascular Disease Statistics 2017, European Heart Network, Brussels." In: *European Cardiovascular Disease Statistics* (2017). ISSN: 0195668X. DOI: 10.1093/eurheartj/eht356. arXiv: 978-2-9537898-1-2.

[5] T. G. Pickering. "Principles and techniques of blood pressure measurement." In: *Cardiology clinics* 20.2 (2002), pp. 207–23. ISSN: 0733-8651. DOI: 10.1016/j.ccl.2010.07.006.Principles.

[6] D. S. Picone et al. "Accuracy of Cuff-Measured Blood Pressure: Systematic Reviews and Meta-Analyses." In: *Journal of the American College of Cardiology* 70.5 (2017), pp. 572–586. ISSN: 15583597. DOI: 10.1016/j.jacc.2017.05.064.

[7] X. R. Ding et al. "Continuous Cuffless Blood Pressure Estimation Using Pulse Transit Time and Photoplethysmogram Intensity Ratio." In: *IEEE Transactions on Biomedical Engineering* 63.5 (2016), pp. 964–972. ISSN: 15582531. DOI: 10.1109/TBME.2015.2480679.

[8] A. Esmaili, M. Kachuee, and M. Shabany. "Nonlinear Cuffless Blood Pressure Estimation of Healthy Subjects Using Pulse Transit Time and Arrival Time." In: *IEEE Transactions on Instrumentation and Measurement* 66.12 (2017), pp. 3299–3308. ISSN: 00189456. DOI: 10.1109/TIM.2017.2745081. arXiv: arXiv:1812.00544v1.

[9] H. Gesche et al. "Continuous blood pressure measurement by using the pulse transit time: Comparison to a cuff-based method." In: *European Journal of Applied Physiology* 112.1 (2012), pp. 309–315. ISSN: 14396319. DOI: 10.1007/s00421-011-1983-3.

[10] S. S. Franklin et al. "White-Coat Hypertension." In: *Hypertension* 62.6 (Dec. 2013), pp. 982–987. DOI: 10.1161/hypertensionaha.113.01275.

[11] B. Gupta. "Monitoring in the ICU Anaesthesia Update in." In: (), pp. 37–42.

[12] S. A. Magder. "The Highs and Lows of Blood Pressure." In: *Critical Care Medicine* 42.5 (2014), pp. 1241–1251. ISSN: 0090-3493. DOI: 10.1097/CCM.0000000000000324.

[13] J.-F. Augusto et al. "Interpretation of blood pressure signal: physiological bases, clinical relevance, and objectives during shock states." In: *Intensive Care Medicine* 37.3 (2011), pp. 411–419. ISSN: 0342-4642. DOI: 10.1007/s00134-010-2092-1.

[14] B. Lamia et al. "Clinical review: interpretation of arterial pressure wave in shock states." In: *Critical care (London, England)* 9.6 (2005), pp. 601–6. ISSN: 1466-609X. DOI: 10.1186/cc3891.

[15] *Module 4: The Cardiovascular System: Blood Vessels and Circulation*.

[16] G. Mancia et al. "2013 ESH/ESC Guidelines for the management of arterial hypertension." In: *Journal of Hypertension* 31.7 (2013), pp. 1281–1357. ISSN: 0263-6352. DOI: 10.1097/01.hjh.0000431740.32696.cc.

[17] C. VanPutte, J. Regan, and A. F. Russo. *Seeley's anatomy and physiology*. 10th Editi. McGraw-Hill, 2014. ISBN: 978–0–07–340363–2.

[18] M. Briet et al. "Arterial stiffness and pulse pressure in CKD and ESRD." In: *Kidney International* 82.4 (2012), pp. 388–400. ISSN: 15231755. DOI: 10.1038/ki.2012.131.

[19] G. Thomas and D. Rees. "Monitoring arterial blood pressure." In: *Anaesthesia & Intensive Care Medicine* 19.4 (2018), pp. 194–197. ISSN: 14720299. DOI: 10.1016/j.mpaic.2018.02.003.

[20] D. Perloff et al. "Human blood pressure determination by sphygmomanometry." In: *Circulation* 88.5 (1993), pp. 2460–2470. ISSN: 0009-7322. DOI: 10.1161/01.CIR.88.5.2460.

[21] R. H. Bailey. "Aneroid Sphygmomanometers." In: *Archives of Internal Medicine* 151.7 (1991), p. 1409. ISSN: 0003-9926. DOI: 10.1001/archinte.1991.00400070157022.

[22] T. G. Pickering et al. "Recommendations for blood pressure measurement in humans and experimental animals. Part 1: Blood pressure measurement in humans: A statement for professionals from the subcommittee of professional and public education of the American Heart Association cou." In: *Hypertension* 45.1 (2005), pp. 142–161. ISSN: 0194911X. DOI: 10.1161/01.HYP.0000150859.47929.8e.

[23] G. Ogedegbe and T. Pickering. "Principles and Techniques of Blood Pressure Measurement." In: *Cardiology Clinics* 28.4 (2010), pp. 571–586. ISSN: 07338651. DOI: 10.1016/j.ccl.2010.07.006. arXiv: arXiv:1011.1669v3.

[24] S. N. Hunyor, J. M. Flynn, and C Cochineas. "Comparison of performance of various sphygmomanometers with intra-arterial blood-pressure readings." In: *British medical journal* 2.6131 (1978), pp. 159–62. ISSN: 0007-1447.

[25] N. R. Campbell et al. "Accurate, reproducible measurement of blood pressure." In: *CMAJ : Canadian Medical Association journal = journal de l'Association medicale canadienne* 143.1 (1990), pp. 19–24. ISSN: 0820-3946.

[26] C. R. Smith. "The Meaning of the Point of Maximum Oscillations in Cuff Pressure in the Indirect Measurement of Blood Pressure—Part II." In: *Journal of Biomechanical Engineering* 102.1 (1980), p. 28. ISSN: 0148-0731. DOI: 10.1115/1.3138195.

[27] G Drzewiecki, R Hood, and H Apple. "Theory of the oscillometric maximum and the systolic and diastolic detection ratios." In: *Annals of biomedical engineering* 22.1 (), pp. 88–96. ISSN: 0090-6964. DOI: 8060030.

[28] R. K. Whyte et al. "Assessment of Doppler ultrasound to measure systolic and diastolic blood pressures in infants and young children." In: *Archives of disease in childhood* 50.7 (1975), pp. 542–4. ISSN: 1468-2044. DOI: 1167067.

[29] G. P. Seifert. "A portable blood pressure monitor utilizing Doppler ultrasound." In: *Retrospective Theses and Dissertations* (1981).

[30] T. Birch. "Continuous Non-Invasive Blood-Pressure Measurements Problem presented by." In: *Artery* September (2007), pp. 10–14.

[31] G Parati et al. "Comparison of finger and intra-arterial blood pressure monitoring at rest and during laboratory testing." In: *Hypertension (Dallas, Tex. : 1979)* 13.6 Pt 1 (1989), pp. 647–55. ISSN: 0194-911X.

[32] J. S. Eckerle. "Tonometry, Arterial." In: *Encyclopedia of Medical Devices and Instrumentation*. Hoboken, NJ, USA: John Wiley & Sons, Inc., 2006. DOI: 10.1002/0471732877.emd250.

[33] H. Sorvoja and R. Myllyla. "Noninvasive blood pressure measurement methods." In: *Molecular and Quantum Acoustics* 27 (2006), pp. 239–264.

[34] G. L. Pressman and P. M. Newgard. "A Transducer for the Continuous External Measurement of Arterial Blood Pressure." In: *IRE Transactions on Bio-Medical Electronics* 10.2 (1963), pp. 73–81. ISSN: 0096-1884. DOI: 10.1109/TBMEL.1963.4322794.

[35] P. Iaizzo. *Handbook of Cardiac Anatomy, Physiology, and Devices*. Ed. by P. A. Iaizzo. Cham: Springer International Publishing, 2015. ISBN: 978-3-319-19463-9. DOI: 10.1007/978-3-319-19464-6. arXiv: arXiv:1011.1669v3.

[36] E. Topol. *Textbook of interventional cardiology*. Philadelphia, PA: Elsevier, 2016. ISBN: 9780323340380.

[37] P. Hamilton. "Open source ECG analysis." In: *Computers in Cardiology*. IEEE. DOI: 10.1109/cic.2002.1166717.

[38] J. Allen. "Photoplethysmography and its application in clinical physiological measurement." In: *Physiological Measurement* 28.3 (2007). ISSN: 09673334. DOI: 10.1088/0967-3334/28/3/R01.

[39] L. Nilsson, A. Johansson, and S. Kalman. "Respiration can be monitored by photoplethysmography with high sensitivity and specificity regardless of anaesthesia and ventilatory mode." In: *Acta Anaesthesiologica Scandinavica* 49.8 (2005), pp. 1157–1162. ISSN: 00015172. DOI: 10.1111/j.1399-6576.2005.00721.x.

[40] M. Ghamari. "A review on wearable photoplethysmography sensors and their potential future applications in health care." In: *International Journal of Biosensors & Bioelectronics* 4.4 (2018), pp. 195–202. ISSN: 25732838. DOI: 10.15406/ijbsbe.2018.04.00125.

[41] J. Spigulis et al. "Simultaneous recording of skin blood pulsations at different vascular depths by multiwavelength photoplethysmography." In: *Appl. Opt.* 46.10 (2007), pp. 1754–1759. DOI: 10.1364/AO.46.001754.

[42] G. Joseph et al. "Photoplethysmogram (PPG) signal analysis and wavelet de-noising." In: *2014 Annual International Conference on Emerging Research Areas: Magnetics, Machines and Drives (AICERA/iCMMD)*. IEEE, 2014, pp. 1–5. ISBN: 978-1-4799-5202-1. DOI: 10.1109/AICERA.2014.6908199.

[43] M. Elgendi. "On the analysis of fingertip photoplethysmogram signals." In: *Current cardiology reviews* 8.1 (2012), pp. 14–25. ISSN: 1875-6557.

[44] A. Steptoe, H. Smulyan, and B. Gribbin. "Pulse Wave Velocity and Blood Pressure Change: Calibration and Applications." In: *Psychophysiology* 13.5 (1976), pp. 488–493. DOI: 10.1111/j.1469-8986.1976.tb00866.x. eprint: https://onlinelibrary.wiley.com/doi/pdf/10.1111/j.1469-8986.1976.tb00866.x.

[45] F. S. Cattivelli and H. Garudadri. "Noninvasive cuffless estimation of blood pressure from pulse arrival time and heart rate with adaptive calibration." In: *2009 Sixth international workshop on wearable and implantable body sensor networks*. IEEE. 2009, pp. 114–119.

[46] L. Peter, N. Noury, and M Cerny. "A review of methods for non-invasive and continuous blood pressure monitoring: Pulse transit time method is promising?" In: *Irbm* 35.5 (2014), pp. 271–282.

[47] Y. Chen et al. "Continuous and noninvasive blood pressure measurement: A novel modeling methodology of the relationship between blood pressure and pulse wave velocity." In: *Annals of Biomedical Engineering* 37.11 (2009), pp. 2222–2233. ISSN: 00906964. DOI: 10.1007/s10439-009-9759-1.

[48] D. J. Hughes et al. "Measurements of Young's Modulus of Elasticity of the Canine Aorta with Ultrasound." In: *Ultrasonic Imaging* 1.4 (1979), pp. 356–367. ISSN: 01617346. DOI: 10.1177/016173467900100406. arXiv: arXiv:1011.1669v3.

[49] W. Chen et al. "Continuous estimation of systolic blood pressure using the pulse arrival time and intermittent calibration." In: *Medical and Biological Engineering and Computing* 38.5 (2000), pp. 569–574. ISSN: 01400118. DOI: 10.1007/BF02345755.

[50] P. Fung et al. "Continuous noninvasive blood pressure measurement by pulse transit time." In: *The 26th Annual International Conference of the IEEE Engineering in Medicine and Biology Society*. IEEE. DOI: 10.1109/iembs.2004.1403264.

[51] J. Proença et al. "Is Pulse Transit Time a good indicator of blood pressure changes during short physical exercise in a young population?" In: *2010 Annual International Conference of the IEEE Engineering in Medicine and Biology Society, EMBC'10* (2010), pp. 598–601. ISSN: 1557-170X. DOI: 10.1109/IEMBS.2010.5626627.

[52] M. Masè et al. "Feasibility of cuff-free measurement of systolic and diastolic arterial blood pressure." In: *Journal of Electrocardiology* 44.2 (Mar. 2011), pp. 201–207. DOI: 10.1016/j.jelectrocard.2010.11.019.

[53] H. T. Ma. "A Blood Pressure Monitoring Method for Stroke Management." In: *BioMed Research International* 2014 (2014), pp. 1–7. DOI: 10.1155/2014/571623.

[54] M. Kachuee et al. "Cuff-less high-accuracy calibration-free blood pressure estimation using pulse transit time." In: *2015 IEEE International Symposium on Circuits and Systems (ISCAS)*. IEEE, May 2015. DOI: 10.1109/iscas.2015.7168806.

[55] R. Lazazzera, Y. Belhaj, and G. Carrault. "A New Wearable Device for Blood Pressure Estimation Using Photoplethysmogram." In: *Sensors* 19.11 (June 2019), p. 2557. DOI: 10.3390/s19112557.

[56] H. J. Baek et al. "Enhancing the estimation of blood pressure using pulse arrival time and two confounding factors." In: *Physiological Measurement* 31.2 (Dec. 2009), pp. 145–157. DOI: 10.1088/0967-3334/31/2/002.

[57] A. Géron. *Hands-On Machine Learning with Scikit-Learn and TensorFlow: Concepts, Tools, and Techniques to Build Intelligent Systems*. O'Reilly Media, 2017. ISBN: 1491962291.

[58] F. Pedregosa et al. "Scikit-learn: Machine Learning in Python." In: *Journal of Machine Learning Research* 12 (2011), pp. 2825–2830.

[59] G. James et al. *An Introduction to Statistical Learning*. Springer New York, 2013. DOI: 10.1007/978-1-4614-7138-7.

[60] B. Murteira. *Probabilidades e Estatistica - Vol.1*. ESCOLAR EDITORA - GRUPO DECKLEI, 2019. ISBN: 9789725923559.

[61] S. O. Haykin. *Neural Networks and Learning Machines (3rd Edition)*. Pearson, 2008. ISBN: 0131471392.

[62] C. M. Bishop. *Pattern Recognition and Machine Learning (Information Science and Statistics)*. Springer, 2016. ISBN: 1493938436.

[63] I. Goodfellow, Y. Bengio, and A. Courville. *Deep Learning*. http://www.deeplearningbook.org. MIT Press, 2016.

[64] M. Huk. "Backpropagation generalized delta rule for the selective attention Sigma-if artificial neural network." In: *International Journal of Applied Mathematics and Computer Science* 22.2 (June 2012), pp. 449–459. DOI: 10.2478/v10006-012-0034-5.

[65] R. Santos. "Human Crowdsourcing Data for Indoor Location Applied to Ambient Assisted Living Scenarios." Master of Science in Biomedical Engineering. FCT-UNL, 2018.

[66] L. A. Geddes et al. "Pulse Transit Time as an Indicator of Arterial Blood Pressure." In: *Psychophysiology* 18.1 (1981), pp. 71–74. ISSN: 0048-5772. DOI: 10.1111/j.1469-8986.1981.tb01545.x.

[67] C. Poon and Y. Zhang. "Cuff-less and Noninvasive Measurements of Arterial Blood Pressure by Pulse Transit Time." In: *2005 IEEE Engineering in Medicine and Biology 27th Annual Conference*. IEEE, 2005, pp. 5877–5880. ISBN: 0-7803-8741-4. DOI: 10.1109/IEMBS.2005.1615827.

[68] A. M. Carek et al. "SeismoWatch: Wearable Cuffless Blood Pressure Monitoring Using Pulse Transit Time." In: *Proc. ACM Interact. Mob. Wearable Ubiquitous Technol.* 1.3 (Sept. 2017), 40:1–40:16. ISSN: 2474-9567. DOI: 10.1145/3130905.

[69] N. P M et al. "Hemodynamic Interventions for Inducing Blood Pressure Variation in Laboratory Settings." In: June 2018.

[70] C. Carreiras et al. *BioSPPy: Biosignal Processing in Python*. [Online; accessed 22/07/2019]. 2015–.

[71] P. V. Gent et al. "Analysing Noisy Driver Physiology Real-Time Using Off-the-Shelf Sensors: Heart Rate Analysis Software from the Taking the Fast Lane Project." en. In: (2018). DOI: 10.13140/rg.2.2.24895.56485.

[72] "IEEE Standard for Wearable Cuffless Blood Pressure Measuring Devices." In: *IEEE Std 1708-2014* (2014), pp. 1–38. DOI: 10.1109/IEEESTD.2014.6882122.

[73] G. S. Stergiou et al. "A Universal Standard for the Validation of Blood Pressure Measuring Devices." In: *Hypertension* 71.3 (Mar. 2018), pp. 368–374. DOI: 10.1161/hypertensionaha.117.10237.

[74] Y. Kurylyak et al. "Photoplethysmogram-based Blood Pressure Evaluation using Kalman Filtering and Neural Networks." In: May 2013. DOI: 10.1109/MeMeA.2013.6549729.

[75] M. Kachuee et al. "Cuffless Blood Pressure Estimation Algorithms for Continuous Health-Care Monitoring." In: *IEEE Transactions on Biomedical Engineering* 64.4 (2017), pp. 859–869. ISSN: 15582531. DOI: 10.1109/TBME.2016.2580904.

[76] L. Wang et al. "A Novel Neural Network Model for Blood Pressure Estimation Using Photoplethesmography without Electrocardiogram." In: *Journal of Healthcare Engineering* 2018 (2018), pp. 1–9. DOI: 10.1155/2018/7804243.

[77] M. Radha et al. "Estimating blood pressure trends and the nocturnal dip from photoplethysmography." In: *Physiological Measurement* 40.2 (2019), p. 025006. DOI: 10.1088/1361-6579/ab030e.

[78] A. E. Johnson et al. "MIMIC-III, a freely accessible critical care database." In: *Scientific Data* 3.1 (May 2016). DOI: 10.1038/sdata.2016.35.

[79] A. L. Goldberger et al. "PhysioBank, PhysioToolkit, and PhysioNet." In: *Circulation* 101.23 (June 2000). DOI: 10.1161/01.cir.101.23.e215.

[80] X. Xing and M. Sun. "Optical blood pressure estimation with photoplethysmography and FFT-based neural networks." In: *Biomedical Optics Express* 7.8 (July 2016), p. 3007. DOI: 10.1364/boe.7.003007.

[81] M. A. Little et al. "Using and understanding cross-validation strategies. Perspectives on Saeb et al." In: *GigaScience* 6.5 (Mar. 2017). DOI: 10.1093/gigascience/gix020.

Appendix

Acquisition Protocol

Fraunhofer
PORTUGAL

"Remarkable Technology, Easy To Use"

Data acquisition Protocol for Cuffless Blood Pressure Estimation

Material

1. PC with Bluetooth Interface;
2. Disposable or Reusable electrodes;
3. AND blood pressure meter;
4. Low cost system (Bitalino, BVP sensor, ECG sensor and cable);
5. Medical grade system (HUB + ECG sensor + BVP sensor+ wrist blood pressure meter);
6. Contact Gel.

System Setup

Both systems use Bluetooth interface to connect with the computer, therefore two different interfaces or PCs are needed to acquire data simultaneously with both systems.

Medical grade system

1. Connect the ECG sensor, the BVP sensor to the HUB ports 1and 2 respectively;
2. Press the ON/OFF button;
3. In the PC Bluetooth settings, pair the device "BiosignalPlux", if necessary use the code "123" (One time step);
4. Open OpenSignals software;
5. Go to "Find and configure your device";
6. Select the correct device, sample frequency of 1000 Hz, channels 1 and 2 and the respective sensor in each channel;
7. The system is now ready to use.

Low Cost System

1. Connect the ECG cable (port on the same side of the BVP sensor cable);
2. Turn the device ON;
3. Pair the device "bitalino" with the PC, if necessary use the code "1234";

4. Open OpenSignals software;
5. Enable the device, and select the port 3 and 5 with sample frequency of 1000 Hz;
6. The system is now ready to use.

Acquisition Procedures

The data acquisition procedure consists in four parts (calibration, static test, test with blood pressure changes and test after a period of time), all of them should be performed in a room with no external disturbing influences and at room temperature.

The same data will be collected using two different devices, a low cost device and a medical grade device

Calibration

1. Place the A&D automatic BP meter cuff in the left arm of the subject, approximately at heart level. Tight it enough to not fall, but without disturbing the normal blood flow.
2. Place both BVP (PPG) sensors in the right arm index and middle fingers, the sensor should not compress to much the tissue, since this can lead to no signal detection.
3. Clean the skin with alcohol and place the ECG electrodes from both devices as shown in the figure bellow. The Driven Right Leg Circuit electrode is optional, but should be used when possible, since it improves signal quality.

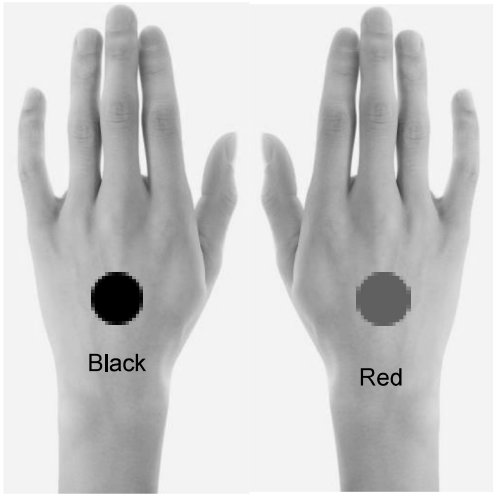

4. The observer should evaluate the ECG and BVP signals quality.

Important Note: The proximity with power sources and charging devices can influence negatively the signals. Due to this factor the device should not be near this electric components.

5. Start the signals recording. During the signal acquisition the subject must be properly sited and with both feet on the ground.
6. Measure the blood pressure 5 times. The measurements must be at least 30 seconds apart to prevent venous congestion. During the process of inflation and deflation of the cuff the subject should stay as still as possible and should not talk.
7. Then the subject must execute a right leg extension while sited until muscle fatigue. During this time the observer should perform as much BP measurements as possible, with the same care mentioned in point 6.
8. Save the data files in .txt format in the subject folder with the format "calibration_A" or "calibration_B", A: Medical grade system and B:low cost system.

Static test

1. The subject should rest for 10 minutes;
2. Maintaining the same setup from calibration, measure 3 times the Blood Pressure with the A&D meter. The measurements must be at least 30 seconds apart;
3. Save the data files in .txt format in the subject folder with the format "staticTest_A" or "staticTest _B", A: Medical grade system and B:low cost system.

Test with BP variation

1. Maintaining the same setup from static test, perform 3 blood pressure measurements with A&D meter, while the subject is doing an isometric exercise (one leg extension as in calibration procedure) until fatigue.
2. Save the data files in .txt format in the subject folder with the format "bpVariation_A" or "bpVariation _B", A: Medical grade system and B:low cost system.

Test after 1 week

1. Repeat the static test
2. Save the data files in .txt format in the subject folder with the format "time _A" or "time _B", A: Medical grade system and B:low cost system.

ANNEX I

Pre Acquisition Questionnaire

Fraunhofer PORTUGAL

Nº _____

"Remarkable Technology, Easy To Use"

Questionário pré-aquisição

Nome: _____

Data Nascimento ___ /___ /_____

Problemas Cardiovascular: ☐ Sim ☐ Não Quais? _____

Medicação: ☐ Sim ☐ Não Quais? _____

Fumador: ☐ Sim ☐ Não

Ingeriu alimentos/bebidas com cafeína (Chá/Café/Bebidas energéticas) nas últimas 6h: ☐ Sim ☐ Não

Ingeriu bebidas alcoólicas nas últimas 6h: ☐ Sim ☐ Não

A preencher pelo observador:

Dia da 1ª medição: ___ /___ /_____ Hora de início da 1ª medição: ___ h ___ min

Dia da 2ª medição: ___ /___ /_____ Hora de início da 2ª medição: ___ h ___ min

Altura: _____ m Massa: _____ Kg

Valores Normais de Pressão Arterial: SYS: _____ mmHg DIA: _____ mmHg

Rua Alfredo Allen 455
4200-135, Porto – PORTUGAL
www.fraunhofer.pt